# Department of Precision and Microsystems Engineering

## Magnetorheological Fluid Damper for Tunable Dampining in Active Mechanical Metamaterials

Samer Habbal


| | |
|---|---|
| Report no | : 2024.006 |
| Coach | : Dr.Andres Hunt |
| Professor | : Dr.Andres Hunt |
| Specialisation | : Mechatronics System Design (MSD) |
| Type of report | : Master Thesis |
| Date | : 31 January 2024 |


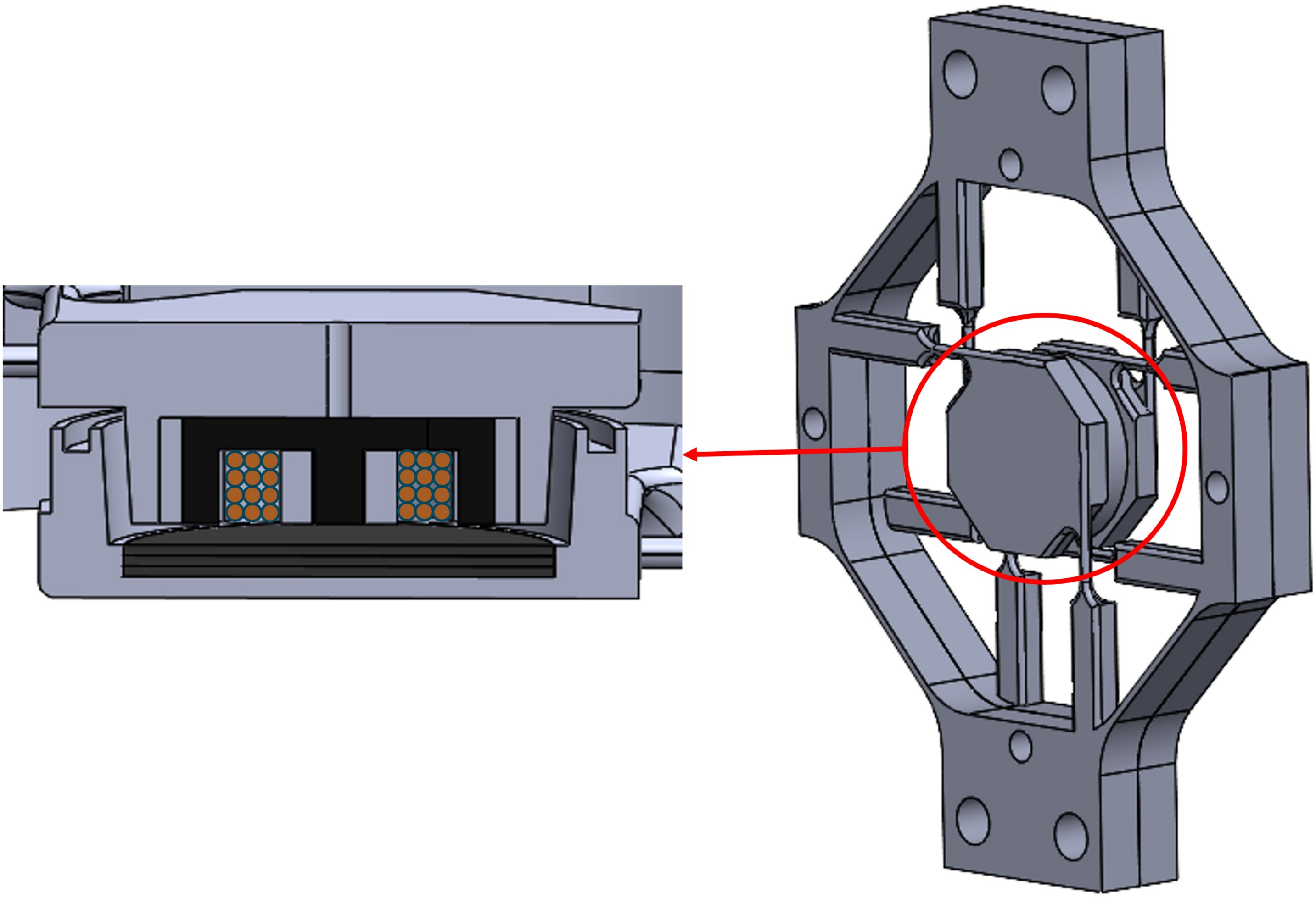

# Magnetorheological Fluid Damper for Tunable Damping in Active Mechanical Metamaterials

by


## Samer Habbal


to obtain the degree of Master of Science

at the Delft University of Technology,

to be defended publicly on Wednesday January 31, 2024 at 10:00 AM.



| | | |
|---|---|---|
| Student number: | 4700880 | |
| Thesis committee: | Dr. ir. A. Hunt, | TU Delft, supervisor |
| | Dr. ir. R. A. J. Ostayen, | TU Delft |
| | Ir. E. P. Ronaes, | TU Delft |

# Contents

# Preface

As I pen down this thesis, it marks the culmination of an intellectual journey into the dynamic realm of active mechanical metamaterials. My fascination with materials that can adapt their mechanical properties in real time fueled the inception of this research endeavour.

Coming from a background in mechanical engineering, I sought to bridge theoretical knowledge with practical applications. The integration of magneto-rheological dampers into active mechanical metamaterials emerged as the focal point of my exploration.

This academic pursuit has not only been a scholarly endeavor but also a personal odyssey of growth, challenges, and triumphs. Guided by the desire to contribute meaningfully to the field of materials science and engineering, I embarked on a journey that unfolded through meticulous design, complex simulations, and hands-on experimentation.

I owe a debt of gratitude to my primary advisor, Dr. Andres Hunt, whose mentorship provided the necessary compass, steering me through the complexities of this research. Dr. Hunt's expertise and commitment to academic excellence have been a beacon of inspiration.

I would also like to acknowledge the influence of Dr. Hassan Hossein Nia, whose contributions enriched the theoretical underpinnings of this work. Special thanks to Gerben van der Meer for his insightful guidance on MR fluid analysis, and Marcin for his hands-on support during the experimental phase.

Beyond the academic arena, my appreciation extends to my wife, Hiba, and my family. Their unwavering support has been my rock, fostering an environment where academic pursuits could thrive. I dedicate this work to the memory of my late father, whose enduring spirit and encouragement echo in these pages.

This thesis reflects not only the technical findings but also the passion, perseverance, and collaborative efforts that have shaped it. May it stand as a testament to the spirit of exploration and a humble contribution to the ever-evolving landscape of materials science.

# Acknowledgments

I am deeply grateful to Dr. Andres Hunt for his invaluable guidance and support throughout the development of this research. His insightful feedback and mentorship have been instrumental in shaping the course of this study. Dr. Hunt's commitment to excellence has consistently inspired me to set ambitious yet achievable goals and has significantly contributed to the success of this thesis.

I would also like to extend my sincere thanks to Dr. Hassan Hossein Nia for his constructive feedback, which has greatly enriched the depth and scope of this research. Dr. Hossein Nia's expertise and encouragement have been pivotal in refining the theoretical aspects of this work.

Special appreciation is extended to Gerben van der Meer, a dedicated PhD student, for his generous assistance in elucidating the complexities of MR fluid and providing invaluable insights into analytical and finite element analysis techniques. His expertise has been a cornerstone in understanding the intricacies of this research domain.

I am indebted to Marcin Kaczmarek for his indispensable contributions to the experimental phase of this study. His assistance in conducting vibration experiments and subsequent data analysis has been pivotal in validating the theoretical findings.

A heartfelt thank you goes out to the Technical Support Staff for their unwavering assistance in the experimental phase. Their dedication to providing technical support during the execution of experiments has ensured the seamless progression of this research, validating the theoretical findings through practical application.

In addition to my academic mentors, I want to express my deepest appreciation to my wife, Hiba, whose unwavering support, understanding, and encouragement sustained me throughout this journey. Her patience and belief in my abilities were my pillars of strength.

I am profoundly grateful to my entire family for their unyielding support. In particular, I want to dedicate this work to the memory of my father, who passed away during the course of this research. His resilience and courage in the face of illness were a source of inspiration. Though he is not here to witness the completion of this thesis, his enduring spirit will forever be a driving force in my academic pursuits.

I am thankful to all my family members for their encouragement and sacrifices and to my friends for their understanding during the challenging phases of this academic endeavour.

This achievement is as much theirs as mine, and I carry their support with me as I progress in my academic and professional journey.

# 1 Introduction

In the rapidly evolving landscape of material science and engineering, the quest for innovative materials with dynamic, adaptive, and tunable properties has become paramount. The demand for such materials spans diverse fields, from medicine to aerospace and automotive industries, where the need for tailored solutions to meet specific application requirements has intensified. This demand has led to the emergence of Mechanical Metamaterials (MMs), a class of materials defined by their unique mechanical properties derived from intricate structures rather than conventional components [1].

While MMs offer a wide range of properties, their inherent limitation lies in the fixed characteristics determined during the initial design. However, Active Mechanical Metamaterials (AMMs) represent a groundbreaking shift in this paradigm. By integrating sensors and actuators within unit elements, AMMs introduce centralized and/or localized control over the distribution of material properties and states within the lattice [3]. This innovation imparts a dynamic and adaptive nature to mechanical metamaterials, allowing for tunable and responsive material properties.

The current state of AMM research is characterized by a diversity of approaches. Previous studies have explored stimuli such as thermal and pneumatic actuation, realizing varying degrees of success. Noteworthy advancements include programmable elastic AMMs utilizing electromagnets for individual control over unit cell stiffness [2]. Other concepts aim to achieve dynamic control over material configuration and dynamic states through embedded piezoelectric stack actuators [3]. The AMM structure comprises nodes or "masses" connected through springs and dampers. Incorporating actuators into this structure makes it possible to adjust the stiffness and damping characteristics over the state of the materials. Our innovative approach involves integrating Magnetorheological Fluid (MRF) dampers into AMMs, effectively addressing Coulomb friction's limitations. MRFs are smart fluids that contain magnetically responsive particles suspended in a liquid carrier. This allows for a dynamic and tunable element that enhances the material's adaptability. The fusion of AMMs and MRF dampers promises unprecedented adaptability, opening doors to applications where precise, on-the-fly adjustments of material properties are essential.

This thesis report documents the exploration of Active Mechanical Metamaterials (AMMs) and their integration with Magnetorheological (MRF) dampers is documented in this thesis report. The report unfolds several key sections, beginning with an introductory chapter that sets the stage for the research. The literature review Chapter 2 provides a comprehensive overview of the current landscape of active mechanical metamaterials, contextualizing the research within existing knowledge. The heart of this thesis resides in Chapter 3, where the intricacies of the Active Mechanical Metamaterials unit cell with an embedded magneto-rheological damper are unveiled. Design considerations, analytical modelling, Finite Element Method (FEM) modelling, dynamic simulation using Simulink, and rigorous experimental validation constitute the core components explored in this chapter. Following the exposition of findings, Chapter 4 draws conclusive remarks. Chapter 5 extends beyond conclusions to reflections on the research process and recommendations for future work. Appendices, including detailed technical drawings, supporting material, and essential data sheets, complement the main chapters.

# 2

# Literature Review - Active mechanical metamaterials

The literature survey investigates various configurations of mechanical metamaterials (MMs) and explores their properties. It particularly focuses on the emerging field of active mechanical metamaterials (AMMs), which combine MMs with smart materials for tunable mechanical structures. The state of the art in AMMs is limited, and the survey emphasizes the need for extensive research to achieve real-time control of AMM properties.

# Active mechanical metamaterials

Samer Habbal

*dept. Precision and Microsystems Engineering*
*Delft university of technology*
Melkweg 2, 2628CD, Delft, the Netherlands
s.habbal@tudelft.nl

***Abstract*—Mechanical metamaterials (MMs) are artificial structures with exotic properties not found in natural materials. The development of MMs has been made possible due to the advancement of additive manufacturing and the widespread use of 3D printers, which has resulted in extensive research investigating MMs and their potential applications. Active mechanical metamaterials (AMMs) are a new class of MMs that can change their mechanical properties in real-time using various stimuli, such as heat, light, electricity, and magnetism. The development of AMMs has the potential to revolutionize the fields of robotics, aerospace, and medical devices by enabling structures with tunable mechanical properties. However, the current state of the art of AMMs is limited by bulky and slow actuators.This literature review aims to investigate the different configurations of AMMs and the properties associated with each one. In addition, it aims to explore the recent advances in smart materials and how they can be integrated with AMMs to achieve mechanical structures with tunable properties. The main findings of this literature review suggest that while the development of AMMs is still in its infancy, recent advancements in smart materials, micro-fabrication techniques, and control algorithms have opened up new avenues for designing structures with unprecedented mechanical properties. However, more research is needed to overcome the current limitations of AMMs and fully realize their potential in various applications.**

***Index Terms*—Metamaterials, Mechanical metamaterials, cellular, Lattice, Origami, chiral, Active metamaterials, Shape memory Polymers, and Magnetorheological fluid.**

## I. Introduction

Metamaterials are engineered structures that aim to attain properties that are different from the constituent material properties, and usually, the intention is to acquire properties that are impossible in nature. The name of this material corresponds to this definition; namely, In Greek, "Meta" means "something beyond " [1], [10]. Materials properties such as electrical permittivity, magnetic permeability and index of refraction are perpetually positive in natural materials such as glass and diamond [10], mechanical constitutive coefficients of natural materials such as stiffness and Poisson's ratio are essentially positive; in contrast, the negative coefficients have been achieved with the design of such metamaterials. From the perspective of application fields and disciplines, metamaterials can be divided into electromagnet metamaterials, acoustic metamaterials, optical metamaterials, and mechanical metamaterials (MMs) field is the most recent field application of metamaterials. This paper will mainly focus on MMs and classify and illustrate them.

Active mechanical metamaterials (AMMs) are a novel class of mechanical materials designed to exhibit real-time controllable mechanical properties. These materials can change their mechanical properties, such as stiffness, damping, and shape, in response to external stimuli, such as temperature, pressure, and electric or magnetic fields. The need for materials with tunable mechanical properties for various applications, such as robotics, aerospace, and civil engineering, drives the development of AMMs. The field of active mechanical metamaterials is still in its infancy, and there is much research to be done to realise these materials' potential fully.

This literature survey aims to investigate the different configurations of mechanical MMs and the properties associated with each one. In addition, research the new field of MMs, which combines the MMs configurations and smart materials to achieve mechanical structures with tunable properties. The ultimate goal of this literature review is to provide insights into the future development of AMMs and their potential applications in various fields.

This paper commences by providing an overview of metamaterials and delving into their intricate history (I-1), with a specific emphasis on mechanical metamaterials (II). The exploration of mechanical metamaterials extends to understanding their structures (II-A) and the associated elastic constants (II-B). The classification of mechanical metamaterials (Section III) includes extreme anisotropic mechanical metamaterials (III-A), auxetic mechanical metamaterials (III-B), mechanical metamaterials with negative properties indices (III-C), and ultra-properties mechanical metamaterials (III-D). As the narrative narrows its focus to Active Mechanical Metamaterials (IV), this paper aims to enrich the evolving landscape by offering a comprehensive exploration of their classifications, properties, and potential applications. The journey into the realm of AMMs unfolds through the examination of Thermal-response AMMs (IV-A), Chemical-response AMMs (IV-B), Pneumatic AMMs (IV-C), those embedded with electro-responsive actuators (IV-D), and those featuring magneto-responsive elements (IV-E). The ensuing discussion (V) critically analyzes the current state of active mechanical metamaterial research, highlights key findings, and addresses potential challenges and future directions in the field. Finally, the paper concludes (VI) by summarizing the key insights gleaned from the exploration of mechanical metamaterials and AMMs.

*1) History of metamaterials:* The first attempt to design a lattice emerged by Newton when he was describing sound propagation in air, and it continues with Rayleigh, who was studying alternating structures. [3]. In 1898, Jagadish Chandra Bose conducted the first microwave experiment on twisted structures [1]. However, the origin of metamaterials was in the field of electromagnetism. Early ideas can be traced back to 1967 when the Russian physicist Veselago hypothesized the ability to make a flat lens and claimed that radiation from a source on one side of a negative index plate could be focused on the other side [11], [12]. In 2000, Smith et al. demonstrated the negative permeability and the negative permittivity by a periodic array of split-ring resonators for the first time. This demonstration started the current interest in metamaterials [15]. Since then, various concepts and devices have been devised that challenge conventional physical laws, such as negative refraction [16], the perfect lens [17], [18], and invisibility cloaking in electromagnetism and optics [19], [20]. The next round of development was in acoustic metamaterials [21] utilizing the principle of local resonance [22]. Sub-wavelength structures opened huge possibilities, including negative effective elastic modulus, negative density, or both. The mechanical metamaterials (MMs), this article's main topic, have evolved within the last few years following the footsteps of the electromagnetic and acoustic metamaterials [14]. The intense research of the previous few years has led to novel inventions in the metamaterials field, for instance, ultralight, ultra-stiff MMs [23], metamaterials with vanishing shear modulus such as pentamode MMs [24], negative refraction elastic waves [25], elastic cloaking [26] and hyperbolic elastic MMs [27].

## II. MECHANICAL METAMATERIALS

Mechanical metamaterials (MMs) have unique mechanical properties based on their structures instead of conventional components. As mentioned in the introduction, metamaterials were initially utilized in optics and electromagnetism. However, the MMs have been developed in the last few years because of the development of additive manufacturing technologies and the widespread use of 3D printers, which facilitated fabricating materials with arbitrarily complicated micro/nano architecture. In this section, the mechanical metamaterials will be discussed in detail, where their structure and the mechanical properties associated with their design will be illustrated. Furthermore, they will be classified, and each category will be demonstrated.

### *A. Structures of mechanical metamaterials*

The structure of the MMs could be a lattice structure or an origami/kirigami structure; in the following section, both will be explained in more detail. The structure of cellular materials, lattice structure, consists of unit cells assembled to fill the space of the material; these unit cells consist of struts "or rods" that form such edges of the network of the structure. The scale of the unit cell can be altered from nm s up to mm s. Cellular structures are initially inspired by natural structures such as honeycombs, sponges, cork, and coral. Understanding these structures is the primary tool for designing and developing the MMS. On the other hand, origami is the art of paper folding associated with Japanese culture. Origami is the term for the art of folding and shaping a flat, square sheet of paper into a finished artwork. In contrast, kirigami refers to creative paper cutting, which starts with a folded base cut, then the finished design is then made by opening and flattening the sheet. Several researchers have been inspired by this creative art to investigate novel MMs. The main idea is to design the structure's unit cells and replicate them with a specific configuration to achieve the final structure with the desired properties. It is also possible to design a structure of multi-scales or hierarchical configuration that can be optimized for a specific application.

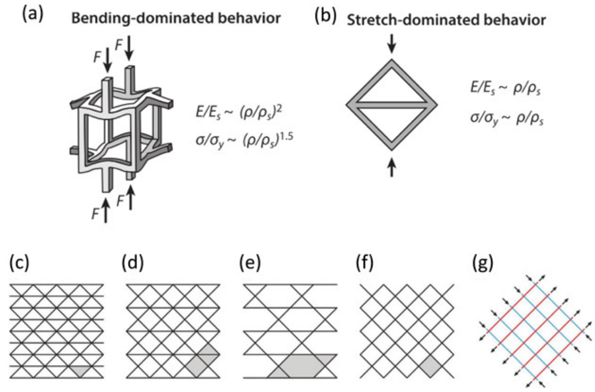


Figure 1. Bending-dominated and stretching-dominated structures a) and b) present the relationship between the mechanical properties and the relative density, c),d) and e) are stretching-dominated structures, f) is bending dominated-structure, g) illustrates the lead case of a fully stretching structure

The most common architecture of the unit cells can be distinguished into two types: bending-dominated structures and stretching-dominated structures [33]. The topological configuration of the structure determines if it is bending or stretching-dominated. The bending-dominated structures are generally deformed by bending the struts or rods of the unit cell, and they are accordingly complaint. In contrast, stretching-dominated structures are deformed through uniaxial tension or compression of the unit cell's struts; for this reason, they are stiffer than bending-dominated structures. Figure (1) exhibits several examples of cellular structures and distinguishes between bending and stretching-dominated structures; moreover, it shows the dimensionless relationship between the mechanical properties and the relative density of the cellular structure. The stretching-stretching configuration can be utilized for the highest specific strength and stiffness, whereas the bending-bending structure can be used for the highest compliance; on the other hand, bending-stretching and stretching-bending configurations can be utilized for intermediate cases.

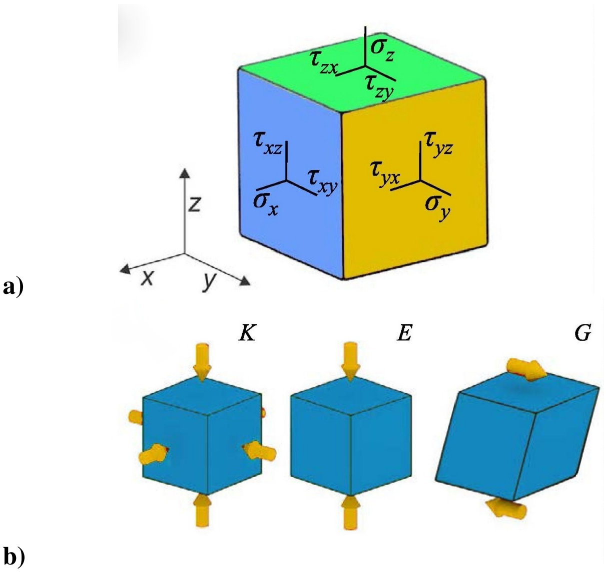


Figure 2. a) The components of normal and shearing stress [4] b) Experimental schemes for measuring compressibility, stiffness and rigidity [4]

*B. Elastic constants associated with mechanical metamaterials*

MMS behaviour is described by four elastic constants [4], namely, the first three constants are the elastic coefficients, and the fourth one is the Poisson's ratio ($\nu$). The elastic coefficients are Young's modulus ($E$), shear modulus ($G$), and bulk modulus ($k$), which correspond respectively to the stiffness, rigidity, and compressibility of structural material. In contrast, Poisson's ratio refers to the deformation of the material perpendicular to the direction of the loading. Figure (2) illustrates an experimental scheme for measuring these constants. In most cases of MMS, it is not easy to measure the elasticity moduli; instead, their elasticity is described by the effective value describes their elasticity since the goal is to deviate them from the bulk material properties [8]

1) Young's modulus($E$): Young's modulus, in some papers, the modulus of elasticity, is a mechanical property that measures the tensile(or compressive) stiffness of the material when it is loaded. It is defined by Hook's law (1) as the ratio of tensile stress ($\sigma$) to tensile strain($\epsilon$). Where stress is the amount of force applied per the unit area ($\sigma = F/A$) and strain is the extension per the unit length ($\epsilon = \Delta L/L$).
$$E = \frac{\sigma}{\epsilon} \tag{1}$$
Young's modulus of a material is a valuable property to predict the material's behaviour under load. In structural materials, when a tensile (or compressive) load acts on the material, it withstands this load by storing it as elastic energy. It returns it when the working load disappears by removing the deformation. When the direction of deformation is in the same direction as the load, the material has a positive stiffness. In contrast, MMS allow for the creation of materials with negative stiffness or, in the same cases, with quasi-zero stiffness.
2) Bulk modulus ($k$): The bulk modulus is a constant that describes how resistant a material is to volume compression. It is described as the ratio between a rise in pressure and the resulting volumetric strain.
$$K = -V\frac{dP}{dV} \tag{2}$$
The minus sign means that when the pressure increases, the volume shrinks. Such a decrease in volume indicates a positive bulk modulus, whereas objects with negative bulk modulus usually tend to expand with an increase in pressure [1]
3) shear modulus ($G$): The shear modulus or the rigidity modulus measures how the material performs under shear stress. The shear modulus ($G$) is defined as the ratio of shear stress ($\tau$) to shear strain($\gamma$).
$$G = \frac{\tau}{\gamma} \tag{3}$$
When the shear deformation is in the same direction as the shear forces, the shear modulus is positive, whereas the negative shear modulus indicates that the direction of the deformation is on the opposite side of the shear forces; furthermore, when the body has no resistance to shear forces, it is referred to as a zero shear modulus.
4) Poisson's ratio ($\nu$): Poisson's ratio is the ratio of the transfer construction strain to the longitudinal extension strain as shown in equation (4).
$$\nu = -\frac{\epsilon trans}{\epsilon long} \tag{4}$$
The minus sign indicates that the materials with a positive Poisson ratio shrink in perpendicular directions when stretched.

## III. Classification of mechanical metamaterials

MMs are artificial materials with unusual mechanical properties that stem from their structures. Developing such metamaterials created various structures with exotic mechanical properties such as zero or negative stiffness, zero or negative Poison's ratio, Negative compressibility, vanishing shear modulus, and structures with unnatural properties. This section will classify the MMs based on the primary elastic moduli and the dimensionless Poison's ratio. Figure (3) illustrates a primary structural classification of MMs. They are divided into four primary groups: Extreme mechanical metamaterials, Auxetic mechanical metamaterials, Negative mechanical metamaterials, and Ultra properties mechanical metamaterials. In addition, the corresponding formulas of the elastic moduli of these different groups are presented.

*A. Extreme anisotropic mechanical metamaterials*

Extreme anisotropic materials were defined in 1995 by Milton and Cherkaev as materials that are highly stiff in some modes of deformation and extremely complaint in some other

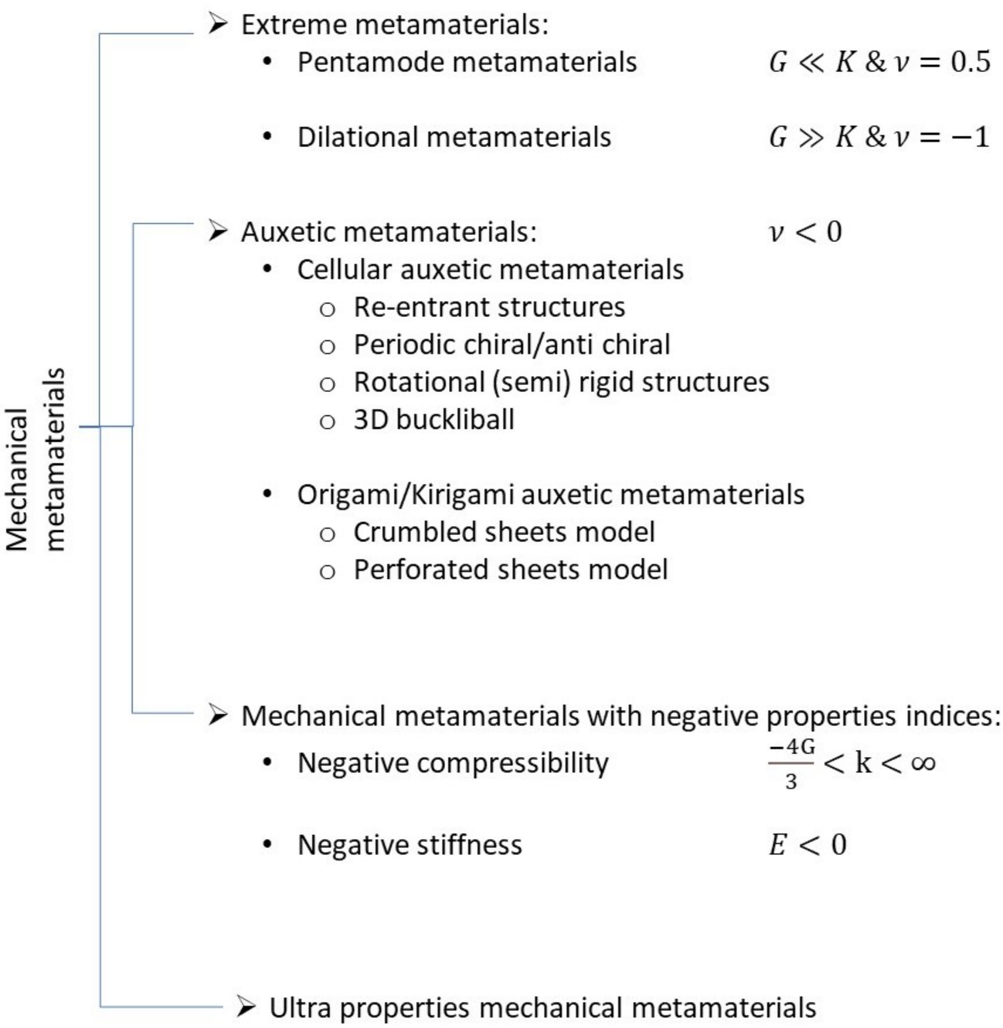


Figure 3. Basic classification of mechanical metamaterials

modes of deformation. Extreme MMs are designated based on their number of modes of deformation where they are highly compliant. Consequently, if the extreme MM has one extremely compliant mode of deformation, it is called unimode MM; if it has two, three, four or five highly compliant modes of deformation, it is called bi-mode, tri-mode, quadramode or penatamode MMs respectively [35]. Two of these categories have received particular attention in the literature: pentamode MMs and a specific case of unimode MMs called dilational metamaterials.

*1) Pentamode mechanical metamaterials:* As mentioned before, pentamode MMs are extremely complaint in five directions, Which means they have very large bulk modulus($K$) compared to their shear modulus ($G$) and the Poisson's ratio of them ($\nu = 0.5$). For this reason, such an MM has a constant volume when it is deformed. Pentamode MMs behave like an ideal fluid because of the very small shear modulus, which is sometimes called meta-fluids [36]. In 1995, Milton and Cherkaev designed ideal pentamode metamaterials with a diamond-like unit cell, which is shown in figure(4a); this unit cell contents of beams with different cross sections connecting in a diamond-like structure [36]. At this time, it was still challenging to be able to manufacture and test such structures. In 2012, Wegener et al., manufactured and tested the diamond-like pentode lattice [36], [41]. This unit cell is shown in figure(4b). After that, Fernandez et al. designed many potential pentamode MMs inspired by Bravias lattices and summarized them in a CAD library available for further researchers [38]. In addition, Zuyu et al. achieved 24 practically realizable pentamode metamaterials without crossing or overlapping bars, which involve isotropic, transversely isotropic and orthotropic structures. In order to achieve that, they applied geometric constraints on the crossing and overlapping of bars; furthermore, they used a ground structure method with a generic algorithm to realize a topology optimization [42].

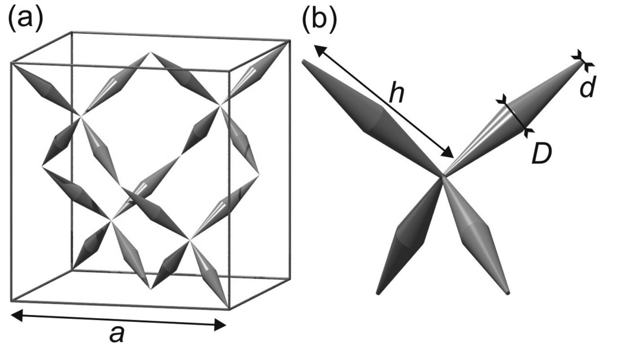


Figure 4. (a) Illustration of the ideal diamond symmetry pentamode MMs suggested by Milton and Cherkaev in 1995 (b) Illustration of the pentamode unite cell developed by Wegener et al. in 2012 [36]

*2) Dilational mechanical metamaterials:* Dilational MM is the opposite case of pentamode MM; in contrast to pentamode MM, the bulk modulus of dilational MM is extremely small compared to its shear modulus. Moreover, it has a Poisson's ratio of ($\nu = -1$). Dilational MM is a particular case of extreme unimode MM, sometimes called compressible materials. When Delational MMs deform, they do not change their shape; the deformation only changes their size. The first Delational MM was defined by Milton in 1991; he developed such a structure with rigid cores and extendable but not bendable beams, and to achieve that, he used the joint content of sliding surfaces [39]. After that, Lakes developed a chiral honeycomb structure with Poisson's ratio equal to -1 [40].

*B. Auxetic mechanical metamaterials*

Auxetic materials are characterized by their negative Poisson ratio. That means when auxetic materials are stretched, they become thicker in the direction perpendicular to the direction of the applied load, which occurs because of the architecture of the material and the way how this structure responds to the uniaxial applied load. Auxetic is derived from the Greek and means "tend to increase". Auxetic materials, in general, could be single molecules or crystals such as $\alpha$-cristobalite structure of Silicon dioxide $Si02$ [44]. They are observed in nature, such as in some human body tissues, certain rocks and minerals, and some polymer's honeycomb structures [45]. In general, the auxetic behaviour can be achieved if the unit cells rotate around the junctions between the unit cells or around the centre of the unit cell. It is also possible to achieve an auxetic behaviour in re-entrant structures: re-entrant refers to something directed inwards or has a negative angle. Auxetic MMs can be divided into two categories: cellular and origami.

*1) Cellular auxetic mechanical metamaterials:*

*a) Re-entrant mechanical metamaterials:* Gibson en Ashby presented in 1982 a cellular re-entrant structure consisting of 2D re-entrant honeycomb unit cells exhibiting auxetic behaviour [46]. Figure(5a) shows the 2D re-entrant hexagon honeycomb composed of curved cell ribs. These curved ribs can reopen under an applied load, leading to an increase in the area of the unit cell and giving the structure an auxetic behaviour. This model has been extended by Masters et al., and they explained that the honeycomb unit cell's deformation could occur in three different mechanisms, namely flexing of the cell ribs, stretching of them or hinging of the junctions between the cell ribs [47]. Moreover, the relationship between the cell properties and the geometry of the cell has been mathematically expressed. They also showed that the regular hexagonal honeycombs are isotropic while the re-entrant honeycombs are highly an-isotropic.
Lakes first produced auxetic materials. He converted a conventional, positive Poisson's ratio foam into auxetic, negative Poisson's ratio one by creating a re-entrant cellular structure through a compression/heating process [48]. Smith et al. have developed a different model of auxetic foam they called the missing rib model [49]. This model, as shown in Figure (5b), has been created by selectively removing some ribs from the unit cell without changing the internal angles and later has been tested by Gaspar et al. [50]. Furthermore, Grima et al. examined the star-shaped structures, which they called "connected stars", and demonstrated the potential of these structures for auxetic behavior [51]. The structures are shown in figure (5c), made from stars of rotational symmetry of 3, exhibiting both auxetic and conventional behaviour, whereas the structures made from stars of rotational symmetry of 4 and 6 exhibit auxetic behaviour. They also showed that the Poisson's ratio is affected by the stiffness of the hinges between the different rods of the structure [51]. Moreover, Overvelde et al. investigated the porous structures and explained the effect of the pore shapes on the properties of the structure [52].

In recent years, some other researchers have been working on designing and developing 3D re-entrant auxetic structures. Yang et al. designed four 3D re-entrant lattice structures and fabricated them using the electron beam melting (EBM) process. Comparing the compressive test results of these different designs, they were able to determine the influence of Poisson's ratio and density on the elastic modulus of the structure; also, they clarified that the 3D re-entrant lattice structure has superior mechanical properties compared to regular foam structures [53]. Bückmann et al. utilized dip-in direct-laser-writing (DLW) optical lithography to fabricate 3D entrant auxetic metamaterials inspired by bow-tie elements [54]. Furthermore, Dong et al. proposed a re-entrant hollow skeleton unit cell and investigated the effects of the material properties and the geometry on the Poisson's ratio of the unit cell [55]. Moreover, Lim et al. have extended the 2D double arrowhead honeycomb structure to a 3D intersecting double arrowhead structure and showed how to control the Poisson's ratio by adjusting the geometry of the unit cell. They also suggested a way to design functionally graded metamaterials where the Poisson's ratio is positive in one plane and negative in the next plane of the structure [58].

*b) Periodic chiral/antichiral:* Chirality refers to an object or system that cannot be superimposed on its mirror. Chirality

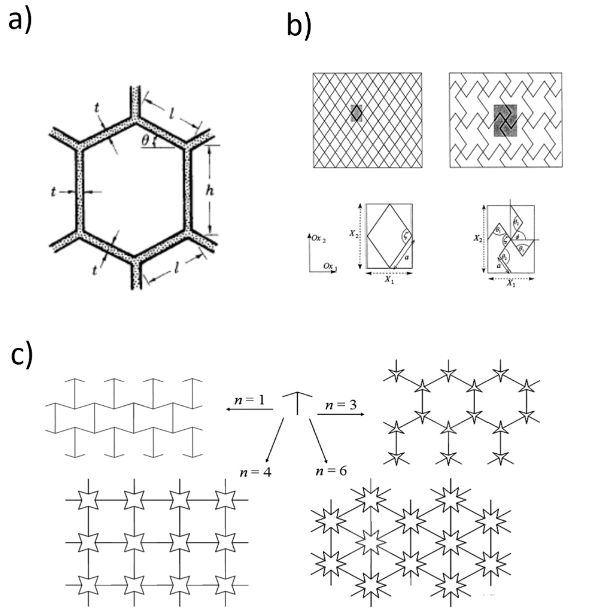


Figure 5. Re-entrant structures a)2D re-entrant honeycomb unit cells [46] b) missing rib foams structure and unit cell [49] c) an auxetic STAR-3, STAR-4 and STAR-6 structures [51]

is commonly observed in nature, such as in right-handed and left-handed sea shells, spiral goat horns, and DNA chiral cellulose. A chiral unit cell consists of a central cylinder attached in tangential alignments, distinguishable from its mirror image, whereas reflexive symmetry is present in anti-chiral systems. Chiral structures are classified into chiral, anti-chiral and meta-chiral structures. Periodic chiral structures can only be created by following the constraints of rotational symmetry; therefore, the number of ligaments attached to each node n results in a rotational symmetry of order n. This results having only five different chiral structures, namely trichirals, anti-trichirals, tetra-chirals, anti-tetrachirals and hexachirals [59], [60] as shown in figure 6.

The properties of such structures depend on the number of ligaments and the length of these ligaments; consequently, the increase of the number of the ligaments increases Young's modulus; furthermore, the tetrachiral and the hexachiral structures are auxetic and have Poisson's ratio close to -1. In contrast, the trichiral structures have a positive Poisson ratio while the anti-trichiral structures have negative Poisson ratios in the structure of short ligaments and positive Poisson ratios in the structure of long ligaments [60]. Furthermore, meta-chiral structures include the basic properties of chiral and anti-chiral structures where within the same structure, there are some nodes which are attached to the same side of the ligaments as in the chiral unit cells and some others attached to opposite sides of the ligaments as in the anti-chiral unit cells, for example of meta-chiral structures is an infinite helical staircase.
Moreover, 3D chiral structures have received some attention

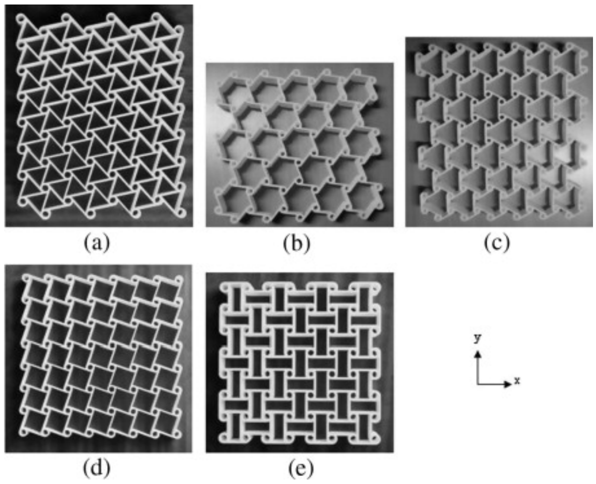


Figure 6. Representative chiral structures (a) hexachiral; (b) trichiral; (c) anti-trichiral; (d) tetrachiral and (e) anti-tetrachiral [60]

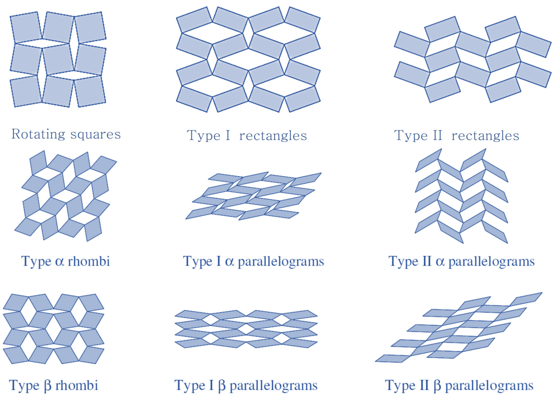


Figure 7. Different types of rotating(-semi) rigid structures [65]

in recent years. Ha et al. developed and analysed a 3D chiral structure consisting of rigid cubical nodules and deformable ribs where Poisson's ratio is geometry-dependent and can be tuned to negative values. The lattices exhibited stretch-twist coupling that increases with the relative slenderness of ribs [61].

*c) Rotation(-semi) rigid structures:* A rotating (semi-) rigid structure consists of rigid squares connected by simple hinges where the squares will rotate at the vertices; hence the structure's stiffness is due to the stiffness of the hinges. The rigid rotating squares could also be rectangles, triangles, rhombi or parallelograms [62] as shown in figure 7.

In general, the Poisson's ratio of such structure depends on the direction of loading. The initial angles between the squares and an idealized rotating squares structure exhibited a constant Poisson's ratio of -1 [65], where the structure of the rotating rectangle shows both positive and negative Poisson's ratio, depending on the angle between the rectangles [63]. Moreover, the structure of rigid rotating triangles also shows positive or negative Poisson's ratio depending on the prevailing deformation, the deformation of the triangle or the rotation of the triangles, which can be varied by changing the shape of the triangles and the angle between them [64]. When the squares are replaced with parallelograms or rhombi, two different structures can be constructed; if the parallelograms/rhombi are attached, the small angle is connected with the big angle of adjacent parallelograms/rhombi, and a space-filling structure is obtained. These structures are designated as type $\alpha$ rotating parallelograms/rhombi. On the other hand, if the parallelograms/rhombi are attached such that like angles of adjacent parallelograms/rhombi are connected to each other, a non-space filling structure is obtained and designated as type $\beta$ rotating parallelograms/rhombi [65]. These structures can also have both negative and positive Poisson's ratio, which depends on the shape of the parallelograms/rhombi, the internal angle of the parallelograms/rhombi, the angle between the parallelograms/rhombi and the direction of loading [65].

*d) 3D Buckliball "or Bucklicrystals":* The buckliball have been introduced by Jongmin et al. and refers to a structure consisting of a periodic arrangement of spherical shells which respond to pressure by decreasing the isotropic volume; this volume reduction is induced by structural transformation caused by the first buckling mode of all alignments. Furthermore, they restricted the number of possible configurations to achieve these foldable structures to five patterns, namely a sphere of 6, 12, 24, 30 or 60 holes, as shown in figure 8 [56], [57].

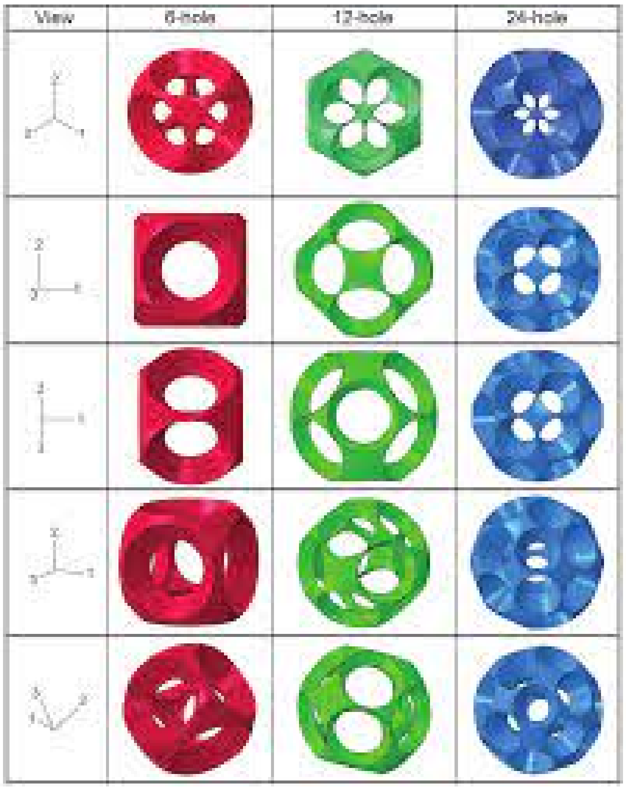


Figure 8. Different views of the building blocks of Bucklicrystals. With 6, 12, and 24 holes. [57]

*2) Origami auxetic metamaterials:* Several researchers have been inspired by the ancient Japanese art of paper folding to investigate novel metamaterials. The concept of paper folding has been extended to include various types of flat materials that could be folded or activated to self-fold to achieve a desired design. Rigid origami has particular importance in MMs where all facets remain unbent, and the creases tend to move like rotating hinges. Miura-ori origami is the most common origami metamaterials tessellation constructed from single repeated parallelogram facets, which are shown in figure 9. Two examples of origami-based metamaterials are presented here for demonstration, and more examples can be found in the literature. Schenk et al. described the deformation of two folded cellular metamaterials based on the Miura tessellation, which exhibited a negative Poisson's ratio for in-plane deformations and a positive Poisson's ratios for out-of-plane one [78]. In addition, Silverberg et al. created metamaterials based on Miura-Ori tessellation with tunable stiffness caused by reversible pop-through defects and facet bending. These defects lead to emergent programmable vacancies and dislocations in the structure [72].

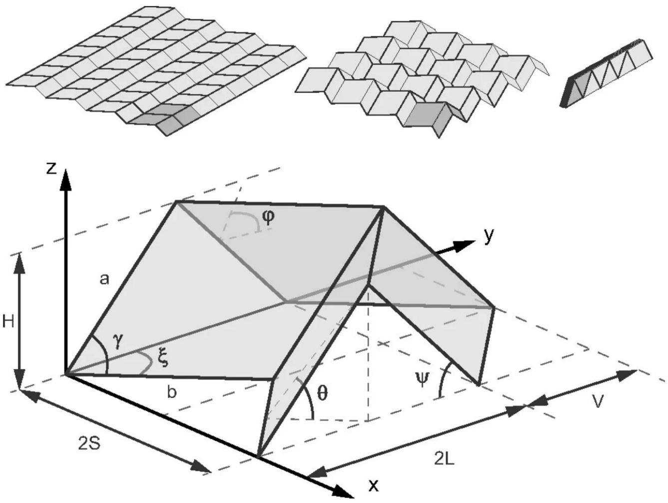


Figure 9. The unit cell geometry of Miura Ori origami mechanical metamaterials [78].

### *C. mechanical metamaterials with negative properties indices*

*1) Negative compressibility mechanical metamaterials:* Materials are usually compressed axially in all directions due to hydrostatic loading. In contrast, materials with negative compressibility expand along a specific axis or plane when loaded hydrostatically. Baughman et al. showed that some rare crystal phases expand in one or more directions when hydrostatically loaded [66], and defined the negative compressibility for the first time. Alomarah et al. showed that negative compressibility could be achieved using bi-material ligaments and clarified that combining two materials with different compressibility cause the negative property [67]. Overvelde et al. presented 2D and 3D truss structures that exhibit negative compressibility; these truss-type structures are composed of rods of different materials connected through pin-joints to form triangular unit cells [68]. In addition, the negative compressibility can be caused by the geometry; for instance, Gaspar et al. modelled 2D hexagonal honeycombs structures with negative compressibility and identified the conditions required to achieve negative compressibility for 2D hexagonal honeycombs and related structures [69]. Furthermore, Grima et al.-2012- modelled a 3D hexagonal dodecahedron with negative compressibility and identified the conditions to achieve the negative compressibility [70]. In addition, Barnes et al. showed that a tetragonal network of nodes connected by bending beams exhibits a negative linear compressibility in one or two directions, where they clarified that the intersecting angle controls the negative compressibility and the optimal intersecting angle resulting in maximum negative compressibility has been reached for both 2D and 3D structures [71].

*2) Negative stiffness mechanical metamaterials:* Materials with positive stiffness deform in the same direction as the applied load and resist that load to return the structure to its previous shape. In contrast, materials with negative stiffness deform in the opposite direction as the applied load and form an auxiliary force that aids deformation [73]. Consequently, materials with negative stiffness experience a more considerable deformation than materials with positive stiffness. On the other hand, negative stiffness structures are assumed to be unstable and have to be stabilized by design. In the literature, there are two ways to stabilize materials with negative stiffness, by combining them with positive stiffness materials or by adding constraints to the structure. By judiciously combining materials with positive and negative stiffness, a composite material with a high stiffness and damping ratio can be obtained, which is desirable for many engineering applications. Lakes et al. experimentally realized the composite approach by embedding negative stiffness inclusions of ferroelastic vanadium dioxide in a metallic matrix of pure tin, resulting in extreme damping and large stiffness [74]. The most common structures in the literature that exhibit negative stiffness behaviour can be designed using buckled elements. Gao et al. presented a negative stiffness metamaterial in which the unit cell consists of cross curve beams, supporting beams and a supporting frame. They showed experimentally that the designed structure exhibits a snap-through behaviour, allowing it to be used in buffering and energy absorption [75]. Zhu et al. designed a bi-material negative stiffness structure that is a combination of soft and hard materials. The fabricated

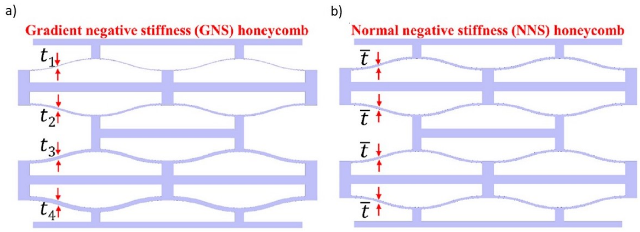


Figure 10. a) 2D model of the honeycomb of gradient negative stiffness metamaterial. b) 2D model the honeycomb of negative stiffness metamaterial. [77]

metamaterial consists of a tube core made of rigid material (PLA) and a soft filling of silicone rubber. Furthermore, a spring is embedded in the unit cell to achieve recoverability and multi-stable characteristics [76]. In addition, Chen et al. proposed a gradient metamaterial with negative stiffness based on curved beams, varying the thickness of the curved beams through the arrangement of the unit cells as shown in Figure (10), a gradient mechanical properties and high specific energy absorption during quasi-static compression have been achieved [77].

### *D. Ultra Properties Mechanical Metamaterials*

Many researchers have been recently trying to develop ultra-stiff, ultra-strong, ultra-tough, and ultralight MMs because these materials with ultra properties are ideal for several applications. Meza et al. created ultra properties MMs composed of nanoscale ceramics shown in figure 11, which are ultra-strong and ultralight. Moreover, they exhibited recoverable deformation after compression over 50% strain [80]. Furthermore, Jang et al. presented ultra-strong metamaterials with a high tensile strength of up to 1.75 GPa without failure, even after multiple deformation cycles. The constituent solids comprise hollow ceramic scaffolds with length scales and hierarchy as biological materials [81]. In addition, Zheng et al. reported MMs with a constant stiffness per unit mass density even when three orders of magnitude reduced the mass density. This structure is a micro-lattice of isotropic unit cells with high structural connectivity and nanoscale features made by projection microstereolithography in combination with nanoscale coating and post-processing [82]. The properties of the created structures are measured, as a function of relative density as shown in figure 12.

## IV. Active mechanical metamaterials(AMMs)

The alteration of the properties of the MMs presented before is almost impossible, and they are mainly evolved for a specific application. Controlling the properties of such materials using added actuators and sensors will enable using them for new applications and, in some cases, in different environmental conditions. Consequently, active mechanical metamaterials (AMMs) can be defined as a combination of mechanical metamaterials

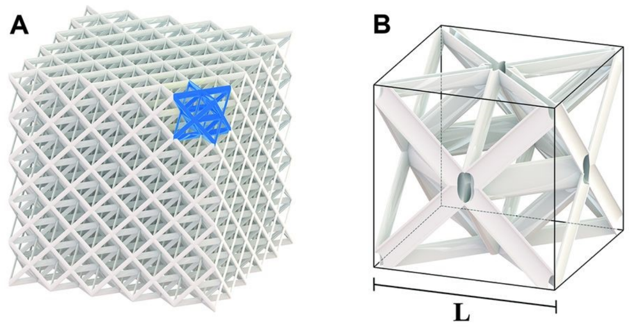


Figure 11. Octet-truss ultra-Strong, ultra-light mechanical metamaterials created by Meza et al. [80]

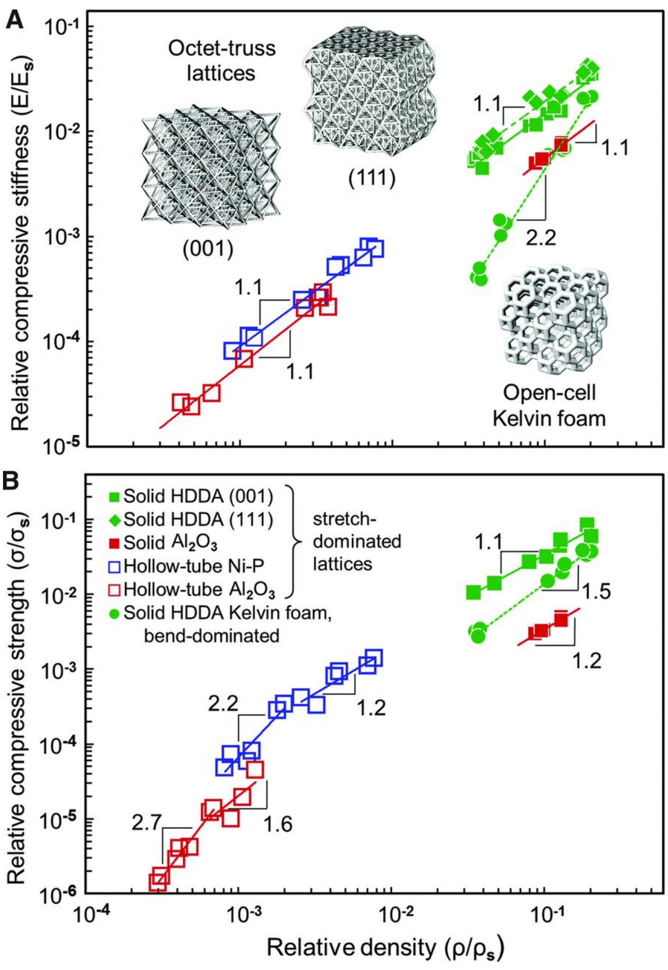


Figure 12. (A) Relative stiffness as a function of relative density for stretch-dominated and bend-dominated micro-lattices. (B) Relative strength as a function of relative density. [82]

and miniaturized integrated actuators to achieve structures with tunable properties. AMMs can be classified according to the kind of stimuli utilized to tune them into different types: t-responsive AMMs, chemical-responsive AMMS, pneumatic (pressure-responsive) AMMs, AMMs with embedded electro-responsive actuators, and magneto-responsive AMMs, as discussed in the following.

### *A. Thermal-response active mechanical metamaterials*

Thermal actuation has been utilized in AMMS for a long time. It is the most common actuation method in AMMS [85], where the properties or the shape of the thermal responsive materials can be controlled by adjusting the temperature. The advantages of thermal-responsive actuation are the high output forces, whereas The disadvantages include the high power consumption, the slow response time, and the dependence on the ambient environment. This actuation method includes different kinds of thermal-responsive materials, shape memory polymers (SMPs) materials, shape memory alloys (SMAs), and liquid crystal elastomers (LCEs). Shape memory polymers (SMPs) are the most common materials to create a thermal responsive AMMS [85]. By combining SMPs with one of the MMs presented in II, a wide variety of thermal responsive AMMs have been developed. The following will present two examples to clarify the principle of utilizing SMPs in thermal-responsive AMMs. Yang et al. developed a lightweight AMMS whose stiffness dropped significantly when its temperature changed from 30 to 90 [83]. The presented structure was able to absorb the shock energy; in addition, they were able to restore the previous original shape and properties even after large deformations. Figure (13a) shows the shape programming through heating, deformation and cooling, and shape recovery to its original shape. Furthermore, Akbari et al. demonstrated two types of structures, a morphing wing flap and a deployable structure where active thermal responsive hinges of SMPs are combined with flexible hinges of elastomeric digital materials shown in figure (13b). The active hinges are actuated using Joule heating generated by resistive wires. This combination of active and flexible hinges is effective in increasing the recovery ratio and the load-bearing capacity of the structure [84].

Shape memory alloys (SMAs) are also popular as actuators for AMMs because they are compliant and can be operated using miniaturized onboard electronics for power and control. Their typical backsides are the long time required for the alloy to cool down and return to its natural shape and compliance. Two examples of using SMAs in thermal-responsive AMMs will be presented. Akbari et al. designed and fabricated different multi-material soft active structures and created various large deformation modes, including twisting, bending and extensional deformation using SMAs wires as actuators, and finally were able to build a soft gripper with an effective grasping and releasing performance [86]. Furthermore, Zhao et al. developed structures with large actuation deformations and high load-bearing capacities [87]. They adjusted the stiffness using SMA springs inside the structure, while the 3D-printed frame provided a large deformation capacity. The structures'

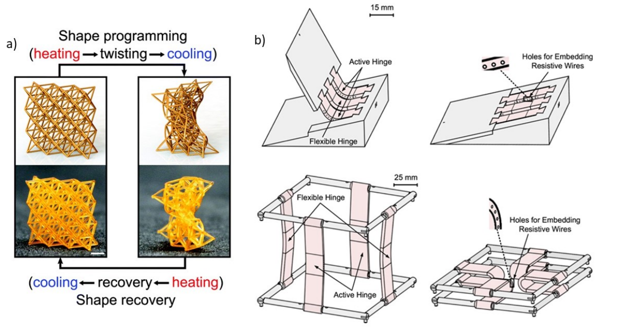


Figure 13. a)shape memory cycle of AMMS based on SMP micro-lattice developed by Yang et al. [83]. b) Programming and actuating steps of the morphing wing flap and the deployable structure created by Akbari et al [84].

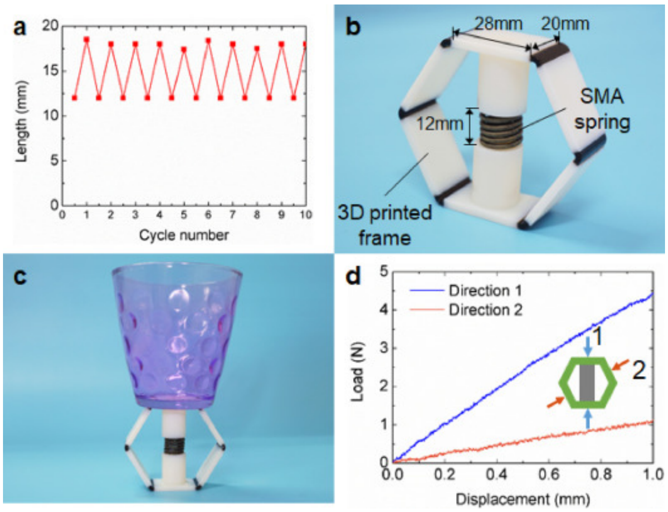


Figure 14. The hexagonal reconfigurable element of AMM with large deformation mode and high load-capacity created by embedding SMAs spring to the 3D printed frame [87].

functions were considerably expanded by changing the load direction and the unit cells' assembly orders as illustrated in figure 14.

Liquid crystal elastomers (LCEs) are also used as thermal responsive materials in AMMS due to their large and reversible deformations when subjected to stimuli. Yuan et al. developed soft actuators with two-way shape-changing behaviour by combining LCEs, 3D printed structures and printed electronics [88]. This actuation principle has been demonstrated by building various active structures, Such as soft morphing aeroplanes, miura-ori, and a sequential folding box. Due to Joule heating produced by the printed conductive wires, the programmed LCE strips bend and lead to the two-way shape-changing behaviour. Moreover, Minori et al. demonstrated a reversible and lightweight actuation method for deployable systems using LCE layers [89]. In addition, Poon et al. introduced an AMM with tunable stiffness by

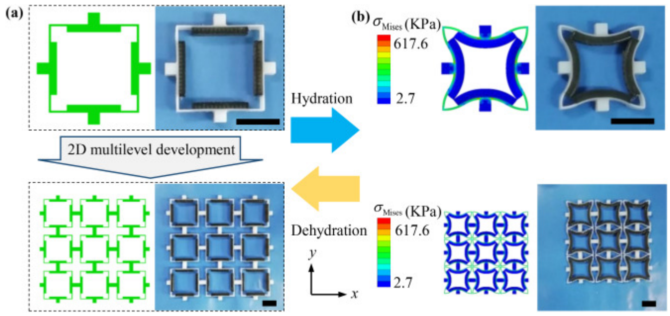


Figure 15. A 2D lattice of chemical-responsive AMM based on the shape-deformation of hydrogels. (a) Initial situation; (b) Deformation situation of finite element and experimental model. [108]

controlling the low-melting temperature of metals embedded in elastomeric. This principle has been illustrated by the structure consisting of a 3D array of Gallium-filled silicone rubber spheres with integrated heater wires that can melt Gallium to reduce the stiffness of the cells [105].

### B. Chemical-response active mechanical metamaterials

Several chemical-responsive AMMS have been developed using various chemical stimuli such as salinity, PH, and humidity. The main downside is that they must be handled in a liquid environment such as in water, acid or organic solvents. Wei et al. presented self-driven auxetic metamaterials based on the shape-deformation of hydrogels. The designed structure has a tunable isotropic negative hydration expansion function where the lattice consists of a hydrogel driving layer and re-entrant auxetic framework as shown in figure 15 [108]. Liu et al. proposed an auxetic AMMS that effectively exhibits a negative swelling behaviour. This structure consists of an array of identical layered plates composed of soft materials that swell when absorbing a solvent. Each double layer has two layers with different swelling properties, resulting in a negative swelling effect [109].

### C. Pneumatic Active Mechanical Metamaterials

In the author's opinion, pneumatic AMMs are also common because of the advantages of reusability and convenience; furthermore, they have a better response time than thermally and chemically responsive ones. On the other hand, when using pneumatic responsive material, altering the structures' properties is limited, and they must be designed for a specific application. In addition, they are very complicated. Chen et al. designed and fabricated AMMS where the stiffness and Poisson's ratio for the pattern transformation could be actuated pneumatically: their structure was composed of elastomers with periodically arranged and interconnected holes. The geometry of these holes can be changed pneumatically, resulting in tuning the properties of the structure [97]. Pan et al. utilized pneumatic actuators to achieve significant and soft bending in flexible metamaterials where the pneumatic chamber is located inside auxetic and non-auxetic metamaterials and causes the structure to bend when inflated [98]. Narang et

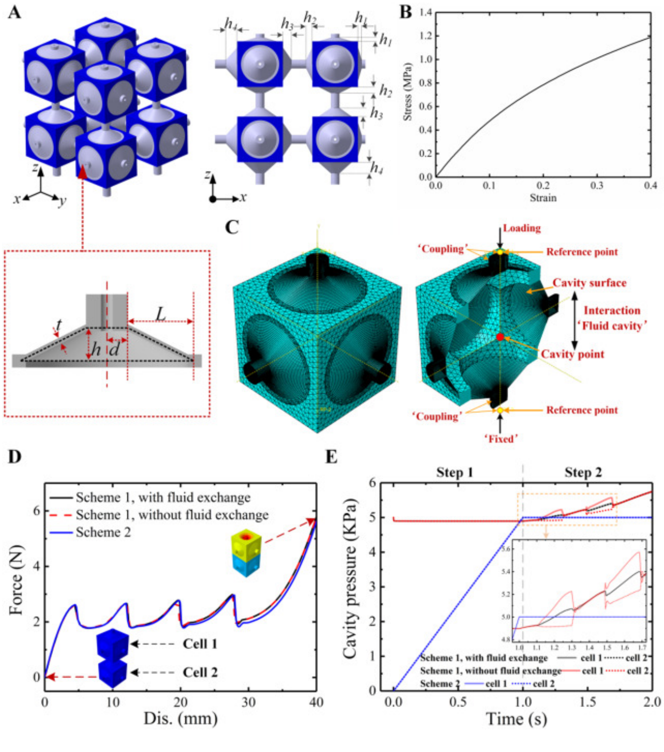


Figure 16. Pneumatically actuated tunable negative stiffness AMMS. (A) Negative stiffness conical shell elements and a cubic supporting structure (B) actual stress-strain response curve of the unit cell's shell element (C) FEM model. [100]

al. designed pneumatic AMMs inspired by laminar jamming, meaning that a laminate of complaint strips is fractionally coupled when a pressure gradient is applied, dramatically changing the mechanical properties. Their structure consists of an acrylic frame containing paper sheets and a vacuum tube where the mechanical properties can be controlled by adjusting the internal pressure through air Inflation or deflation [99]. Tan et al. presented pneumatically actuated tunable negative stiffness AMMS with real-time tunable properties consisting of negative stiffness conical shell elements and a cubic supporting structure as shown in figure 16. They demonstrated that multistage pattern transformation could be realized through pneumatic actuation and showed the influence of the inner air pressure on the mechanical properties and the vibration isolation performance [100].

In addition, Overvelde et al. presented a three-dimensional actuated origami-inspired AMM with multiple degrees of freedom that can alter its shape, volume and stiffness [107]. It consists of rigid faces and pneumatically actuated hinges, which are joined together to create a periodic structure of extruded cubes as shown in Figure 17.

### *D. Active Mechanical Metamaterials with embedded electro-responsive actuator*

Several researchers utilized smart materials actuators to tune the properties of AMMs, aiming to overcome the low response time of the other previously mentioned actuation technologies

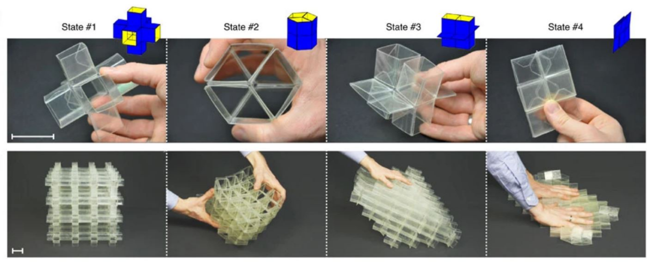


Figure 17. 3D pneumatically actuated Origami-Inspired AMMs [107]

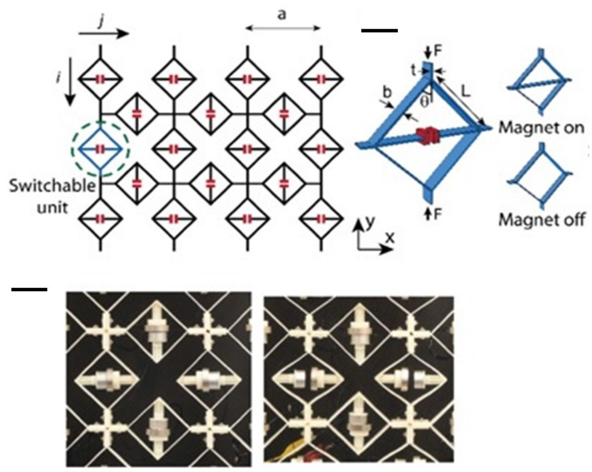


Figure 18. AMMs with Programmable elastic properties based on embedded electromagnets [101]

and achieve real-time active control of the properties of the AMMs. Haghpanah et al. can achieve a programmable elastic AMM by combining the mechanical metamaterial lattice with electromagnets that can lock the strut of the unit cell when switched on, as shown in figure18, which makes it possible to individually control the stiffness of the unit cell and thereby adjust the lattice elastic properties [101].

Thomas created an active unit cell with embedded miniaturized electromagnet actuators to achieve active damping based on electromagnetically altering the coulomb friction. Two variants of unit cells have been fabricated and tested [102]. This structure can be used for limited bandwidth; moreover, it is not dynamically controlled since the actuators cannot force the structure. Saravana Jothi and Hunt make a concept to attain dynamic control over the material configuration and dynamic state. They built AMMs with embedded commercially available piezoelectric stack actuators as shown in Figure (19) [103]. Further research on this structure could make it possible to realize dynamic control over the state of the stress or strain field within the material.

Another attempt in developing electro-responsive materials was to create self-sensing AMMS that continuously senses

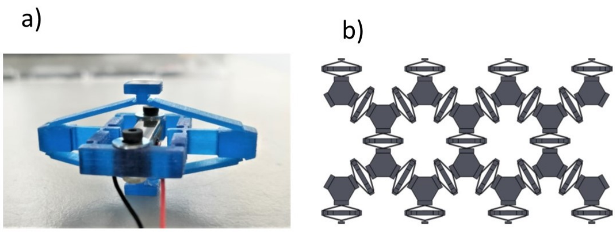


Figure 19. a) An AMM actuation unit with an integrated piezoelectric actuator. b) Interconnecting the actuation units into a hexagonal AMM lattice [103]

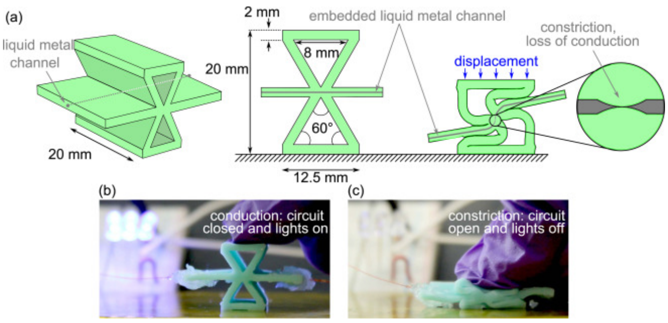


Figure 20. AMM unit cell with liquid metal microchannels as digital sensors [90].

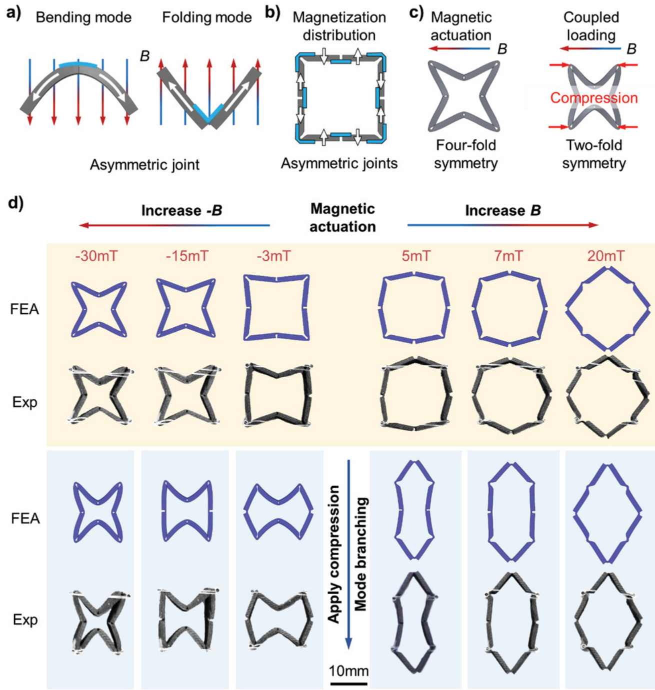


Figure 21. Magneto-Responsive AMM made of Hollow cuboctahedron lattice filled with MRF [92].

the local mechanical deformation of the stressed metamaterials. Nick et al. created the multifunctional AMMs concept [90], which produces digital electrical signals in response to smooth and continuous compressive deformation of buckling components(digital sensor). They designed a structure with micro-fluidic channels filled with liquid metal inside. The deformation of the structure due to a compressive load will result in the deformation of the microfluidic channels resulting in a change in the resistance of the liquid metal as shown in figure 20.

### *E. Magneto-Responsive Active Mechanical Metamaterials*

Magnetorheological materials (MRMs) consist of micron-sized magnetically permeable particles (3 to 5 microns) dispersed in a non-magnetic medium [91]. The rheological properties of these materials are rapidly and reversibly varied when a magnetic field is applied. MRMs can be divided into magnetorheological fluids. (MRFs), magnetorheological elastomers (MREs), and magnetorheological gels (MRGs). MRFs are still limited in AMMS because the MRFS need to be solid, making it challenging to combine them with the configuration of mechanical metamaterials. Jacksoet et al. utilized MRFs filled in hollow cuboctahedron lattices, as shown in figure 21, and demonstrated experimentally that the effective stiffness could be efficiently modified by applying a magnetic field, and they showed that the stiffness could increase 35 % when the structure exposed to a magnetic field of 0.11 T [92].

In contrast to MRF, magnetorheological elastomers (MREs), which consist of a soft elastomer matrix embedded with hard-magnetic particles, are solid and can be combined with the configuration of mechanical metamaterials presented in II. Montgomery et al. demonstrated a magneto AMMS that presents a tunability of the shape and properties utilizing an asymmetric MRE joint, resulting in two modes of deformations depending on the direction of the applied magnetic field, namely bending and folding form. This change in shape also allows for remarkable tunability in properties such as mechanical stiffness and acoustic bandgaps. Kim et al. reported a novel concept to create programmed ferromagnetic AMMS with fast and complex actions driven by magnetic field [93]. They achieved a distribution of magnetic density and orientation by printing MREs under an external magnetic field applied to the dispensing nozzle while printing. Novelino et al. designed and built functional origami-based microrobots with a magneto-responsive plate on the free end of the origami unit cell [94]. This magneto-responsive plate would align with the direction of the external applied magnetic field and allow the origami unit cells to be driven independently. Ma et al. presented the magnetic multi-material printing technology that enables the integrated 3D printing of the magnetic shape memory polymer MSMs where both magnetic and thermal fields can control the deformation. They demonstrated a series of designs with multimodal deformation and tunable Poisson's ratio [95]. Furthermore, Gu et al. developed simple AMMs utilizing small permanent magnets where they proposed a magnetic quadrupole module that can be assembled to form arbitrary

2D shapes with arbitrary magnetizations [96]. To demonstrate this design strategy, they developed the auxetic structures with soft ligaments where the applied magnetic field could program the dynamic deformation of the soft structures. Chen et al. invented a re-programmable AMMS using an arrangement of physical binary elements. Each element consists of a bi-stable, elastic and conic shell, a magnetic cap that drives the shell, two sets of naturally curved columns, two stoppers that amplify the difference in the mechanical behaviour of the two states and a top lid. By controlling these physical binary elements individually using a magnetic signal, the mechanical properties can be changed with stable memory at the unit cell level [104]. Tan et al. introduced an AMM consisting of bistable metamaterial with embedded multiple magnets configured in a mode with an angle equal to $\pi/2$ in order to improve energy trapping property [106].

## V. Discussion

Metamaterials are artificial structures with unnatural properties that started in electromagnetic and optical fields and evolved into mechanical metamaterials that show exotic mechanical properties such as negative stiffness, negative Poisson's ratio, and vanishing shear modulus. These properties are caused by the structure's geometry and configuration instead of the conventional components. AMMS have a broad scope of application fields; for example, in the soft robotic field, Soft robots can be highly durable and secure, yet usually fail to match the strength and precision of rigid robots. This division between soft and rigid has recently started to break down, with emerging research interest in AMMS. Some of AMM's other application fields are presented below. Smart robots, such as smart grippers and smart wearable systems. Miniaturized systems, including microactuators, microfluidic and soft pumps. Aerospace applications, such as smart load-bearing and morphing airfoils. Bio-medicine applications include tissue engineering, drug delivery carriers and electronic skin.

The concept of cellular structure has been introduced previously. However, the recent development of additive-manufacturing technologies or 3D printing has played an essential role in developing mechanical metamaterials with a wide range of sizes of unit cells to nanometer scales. The most advanced structures of mechanical metamaterials have been developed for a specific application. The combination of mechanical metamaterials and smart materials produces the AMMS, which are programmed and tunable, leading to a wide range of new applications.

Active mechanical metamaterials are still in the early development phase, and research in this area is limited. The most currently developed AMMs comprise an elastic main support structure with sensing and driving stimuli-responsive materials. The development of the AMMs requires extreme effort, starting with improving the basic elastic supporting structures, further improving the stimuli-responsive materials used to sense and actuate the structure, and developing the combining design of both. Furthermore, thermal-responsive and chemical-responsive materials can be easily embedded in mechanical metamaterial structures. However, it has a limited application area because they have a slow response time and are affected by the ambient environment. Embedding electro-smart actuators into the AMMS can overcome this problem, but the embedded actuators are still bulky and need to be miniaturized. Developing compact sensors and actuators will make it possible to produce novel types of AMMS that are possible for new application fields. In addition, developing manufacturing technology, such as 3D printing, will also play an essential role in enhancing and developing the AMMs.

## VI. Conclusion

This report aims to investigate mechanical metamaterials and AMMs. Metamaterials and mechanical metamaterials are covered in the introduction I with a brief history of their development. Section II explores the mechanical metamaterials in more detail where their structures and properties are addressed. Furthermore, mechanical metamaterials are classified into different types: Extreme mechanical metamaterials, auxetic mechanical metamaterials, negative mechanical metamaterials with negative properties indices and ultra properties Mechanical Metamaterials. Over the past two decades, mechanical metamaterials have been of particular interest. Furthermore, mechanical metamaterials are made for specific applications with fixed properties. Altering the properties of mechanical metamaterials is impossible since their properties are caused by the geometry and the arrangement of their structure. AMMs can overcome that and allow the structure properties to become tunable and programmable by controlling the added stimuli-responsive materials or the embedded actuators. Furthermore, section IV discusses the AMMS and presents their state of the art; moreover, it shows that the actuation technologies still limit AMMS that can be embedded in them.

Extensive research is needed to obtain real-time control of the properties of the AMMs. It starts with developing new compact intelligent actuators or using different actuation techniques that still need to be considered in the literature. In addition, the design of the unit cell has to be developed to achieve tunability of the properties by embedding compact actuators. One of the actuation techniques that could be used to develop AMMs with new application fields is damping based on tuning the properties of the magnetorheological fluid. Building such a structure will allow the realising of electromagnetically controllable damping for active mechanical metamaterials.

## VII. Acknowledgement

The author would like to thank Dr Andres Hunt for his valuable feedback which regularly guides him to make achievable goals and make a good plan to achieve them.

## References

[1] Navin Shankar Saravana Jothi, "Active metamaterial",2021.

[2] Valipour, Ali, et al. "Metamaterials and their applications: an overview." Proceedings of the Institution of Mechanical Engineers, Part L: Journal of Materials: Design and Applications (2021): 1464420721995858.

[3] Hussein, Mahmoud I., Michael J. Leamy, and Massimo Ruzzene. "Dynamics of phononic materials and structures: Historical origins, recent progress, and future outlook." Applied Mechanics Reviews 66.4 (2014).
[4] Yu, Xianglong, et al. "Mechanical metamaterials associated with stiffness, rigidity and compressibility: A brief review." Progress in Materials Science 94 (2018): 114-173.
[5] Bertoldi, Katia, et al. "Flexible mechanical metamaterials." Nature Reviews Materials 2.11 (2017): 1-11.
[6] Jiao, Pengcheng, and Amir H. Alavi. "Artificial intelligence-enabled smart mechanical metamaterials: advent and future trends." International Materials Reviews 66.6 (2021): 365-393.
[7] Yuan, Xujin, et al. "Recent progress in the design and fabrication of multifunctional structures based on metamaterials." Current Opinion in Solid State and Materials Science 25.1 (2021): 100883.
[8] Barchiesi, Emilio, Mario Spagnuolo, and Luca Placidi. "Mechanical metamaterials: a state of the art." Mathematics and Mechanics of Solids 24.1 (2019): 212-234.
[9] Lee, Jae-Hwang, Jonathan P. Singer, and Edwin L. Thomas. "Micro-/nanostructured mechanical metamaterials." Advanced materials 24.36 (2012): 4782-4810.
[10] Kshetrimayum, Rakhesh S. "A brief intro to metamaterials." IEEE potentials 23.5 (2004): 44-46.
[11] Shamonina, Ekaterina, and L. Solymar. "Metamaterials: How the subject started." Metamaterials 1.1 (2007): 12-18.
[12] Tretyakov, Sergei A. "A personal view on the origins and developments of the metamaterial concept." Journal of Optics 19.1 (2016): 013002.
[13] Fischer, Sarah CL, Leonie Hillen, and Chris Eberl. "Mechanical metamaterials on the way from laboratory scale to industrial applications: challenges for characterization and scalability." Materials 13.16 (2020): 3605.
[14] Zadpoor, Amir A. "Mechanical meta-materials." Materials Horizons 3.5 (2016): 371-381.
[15] Smith, David R., et al. "Composite medium with simultaneously negative permeability and permittivity." Physical review letters 84.18 (2000): 4184.
[16] Shelby, Richard A., David R. Smith, and Seldon Schultz. "Experimental verification of a negative index of refraction." science 292.5514 (2001): 77-79.
[17] Pendry, John Brian. "Negative refraction makes a perfect lens." Physical review letters 85.18 (2000): 3966.
[18] Pendry, J. B. "A chiral route to negative refraction." Science 306.5700 (2004): 1353-1355.
[19] Chen, Huanyang, Che Ting Chan, and Ping Sheng. "Transformation optics and metamaterials." Nature materials 9.5 (2010): 387-396.
[20] Liu, Yongmin, and Xiang Zhang. "Metamaterials: a new frontier of science and technology." Chemical Society Reviews 40.5 (2011): 2494-2507.
[21] Deymier, Pierre A. "Introduction to phononic crystals and acoustic metamaterials." Acoustic metamaterials and phononic crystals. Springer, Berlin, Heidelberg, 2013. 1-12.
[22] Liu, Zhengyou, et al. "Locally resonant sonic materials." science 289.5485 (2000): 1734-1736.
[23] Zheng, Xiaoyu, et al. "Ultralight, ultrastiff mechanical metamaterials." Science 344.6190 (2014): 1373-1377.
[24] Kadic, Muamer, et al. "On the practicability of pentamode mechanical metamaterials." Applied Physics Letters 100.19 (2012): 191901.
[25] Zhu, Rui, et al. "Negative refraction of elastic waves at the deep-subwavelength scale in a single-phase metamaterial." Nature communications 5.1 (2014): 1-8.
[26] Milton, Graeme W., Marc Briane, and John R. Willis. "On cloaking for elasticity and physical equations with a transformation invariant form." New Journal of Physics 8.10 (2006): 248.
[27] García-Chocano, Victor M., Johan Christensen, and José Sánchez-Dehesa. "Negative refraction and energy funneling by hyperbolic materials: An experimental demonstration in acoustics." Physical review letters 112.14 (2014): 144301.
[28] Qi, Jixiang, et al. "Recent Progress in Active Mechanical Metamaterials and Construction Principles." Advanced Science (2022): 2102662
[29] Jin, Binjie, et al. "Programming a crystalline shape memory polymer network with thermo-and photo-reversible bonds toward a single-component soft robot." Science advances 4.1 (2018): eaao3865.
[30] Kelkar, Parth Uday, et al. "Cellular auxetic structures for mechanical metamaterials: A review." Sensors 20.11 (2020): 3132.
[31] Wu, Wenwang, et al. "Mechanical design and multifunctional applications of chiral mechanical metamaterials: A review." Materials and Design 180 (2019): 107950.
[32] Wu, Lingling, et al. "A brief review of dynamic mechanical metamaterials for mechanical energy manipulation." Materials Today 44 (2021): 168-193.
[33] Surjadi, James Utama, et al. "Mechanical metamaterials and their engineering applications." Advanced Engineering Materials 21.3 (2019): 1800864.
[34] Montgomery, S. Macrae, et al. "Recent advances in additive manufacturing of active mechanical metamaterials." Current Opinion in Solid State and Materials Science 24.5 (2020): 100869.
[35] Milton, Graeme W., and Andrej V. Cherkaev. "Which elasticity tensors are realizable?." (1995): 483-493.
[36] Kadic, Muamer, et al. "On the practicability of pentamode mechanical metamaterials." Applied Physics Letters 100.19 (2012): 191901.
[37] Kadic, Muamer, et al. "On the practicability of pentamode mechanical metamaterials." Applied Physics Letters 100.19 (2012): 191901.
[38] Méjica, Graciela Fernández, and Andrés Díaz Lantada. "Comparative study of potential pentamodal metamaterials inspired by Bravais lattices." Smart Materials and Structures 22.11 (2013): 115013.
[39] Milton, Graeme W. "Composite materials with Poisson's ratios close to—1." Journal of the Mechanics and Physics of Solids 40.5 (1992): 1105-1137.
[40] Prall, D., and R. S. Lakes. "Properties of a chiral honeycomb with a Poisson's ratio of—1." International Journal of Mechanical Sciences 39.3 (1997): 305-314.
[41] Schittny, Robert, et al. "Elastic measurements on macroscopic three-dimensional pentamode metamaterials." Applied Physics Letters 103.23 (2013): 231905.
[42] Li, Zuyu, et al. "Topological design of pentamode lattice metamaterials using a ground structure method." Materials and Design 202 (2021) 109523.
[43] Alomarah, Amer. Mechanical Properties of Novel Auxetic Structures. Diss. Swinburne University of Technology, 2021.
[44] Yeganeh-Haeri, Amir, Donald J. Weidner, and John B. Parise. "Elasticity of $\alpha$-cristobalite - a silicon dioxide with a negative Poisson's ratio." Science 257.5070 (1992) 650-652.
[45] Burke, Maria. "A stretch of the imagination." New Scientist 154.2085 (1997): 36-9
[46] Gibson, Lorna J., et al. "The mechanics of two-dimensional cellular materials." Proceedings of the Royal Society of London. A. Mathematical and Physical Sciences 382.1782 (1982): 25-42.
[47] Masters, I. G., and K. E. Evans. "Models for the elastic deformation of honeycombs." Composite structures 35.4 (1996): 403-422.
[48] Lakes, Roderic. "Foam structures with a negative Poisson's ratio." Science 235.4792 (1987): 1038-1040.
[49] Smith, Chris W., J. N. Grima, and KenE Evans. "A novel mechanism for generating auxetic behaviour in reticulated foams: missing rib foam model." Acta materialia 48.17 (2000): 4349-4356.
[50] Gaspar, Neil, et al. "Novel honeycombs with auxetic behaviour." Acta Materialia 53.8 (2005): 2439-2445.
[51] Grima, Joseph N., et al. "On the potential of connected stars as auxetic systems." Molecular Simulation 31.13 (2005): 925-935.
[52] Overvelde, Johannes Tesse Bastiaan, Sicong Shan, and Katia Bertoldi. "Compaction through buckling in 2D periodic, soft and porous structures: effect of pore shape." Advanced Materials 24.17 (2012) 2337-2342.
[53] Yang, Li, et al. "Compressive properties of Ti–6Al–4V auxetic mesh structures made by electron beam melting." Acta Materialia 60.8 (2012): 3370-3379.
[54] Bückmann, Tiemo, et al. "Tailored 3D mechanical metamaterials made by dip-in direct-laser-writing optical lithography." Advanced Materials 24.20 (2012): 2710-2714.
[55] Li, Dong, Liang Dong, and Roderic S. Lakes. "A unit cell structure with tunable Poisson's ratio from positive to negative." Materials Letters 164 (2016): 456-459.
[56] Shim, Jongmin, et al. "Buckling-induced encapsulation of structured elastic shells under pressure." Proceedings of the National Academy of Sciences 109.16 (2012): 5978-5983.
[57] Babaee, Sahab, et al. "3D soft metamaterials with negative Poisson's ratio." Advanced Materials 25.36 (2013): 5044-5049.
[58] Lim, Teik-Cheng. "A 3D auxetic material based on intersecting double arrowheads." physica status solidi (b) 253.7 (2016): 1252-1260.

[59] Grima, Joseph N., Ruben Gatt, and Pierre-Sandre Farrugia. ”On the properties of auxetic meta-tetrachiral structures.” physica status solidi (b) 245.3 (2008): 511-520.
[60] Alderson, Andrew, et al. ”Elastic constants of 3-, 4-and 6-connected chiral and anti-chiral honeycombs subject to uniaxial in-plane loading.” Composites Science and Technology 70.7 (2010): 1042-1048.
[61] Ha, Chan Soo, Michael E. Plesha, and Roderic S. Lakes. ”Chiral three-dimensional lattices with tunable Poisson’s ratio.” Smart Materials and Structures 25.5 (2016): 054005.
[62] Grima, Joseph N., and Kenneth E. Evans. ”Auxetic behavior from rotating squares.” (2000).
[63] Andrew, Alderson. ”Negative Poisson’s ratios from rotating rectangles.” Cmst 10.2 (2004): 137-145.
[64] Grima, Joseph N., and Kenneth E. Evans. ”Auxetic behavior from rotating triangles.” Journal of materials science 41.10 (2006): 3193-3196.
[65] Grima, Joseph N., et al. ”On the auxetic properties of rotating rhombi and parallelograms: A preliminary investigation.” physica status solidi (b) 245.3 (2008): 521-529. triangles.” Journal of materials science 41.10 (2006): 3193-3196.
[66] Baughman, Ray H., et al. ”Materials with negative compressibilities in one or more dimensions.” Science 279.5356 (1998): 1522-1524.
[67] Alomarah, Amer. Mechanical Properties of Novel Auxetic Structures. Diss. Swinburne University of Technology, 2021.
[68] Overvelde, Johannes Tesse Bastiaan, Sicong Shan, and Katia Bertoldi. ”Compaction through buckling in 2D periodic, soft and porous structures: effect of pore shape.” Advanced Materials 24.17 (2012): 2337-2342.
[69] Gaspar, Neil, et al. ”Novel honeycombs with auxetic behaviour.” Acta Materialia 53.8 (2005): 2439-2445.
[70] Grima, Joseph N., et al. ”On the potential of connected stars as auxetic systems.” Molecular Simulation 31.13 (2005): 925-935.
[71] Barnes, D. L., et al. ”Modelling negative linear compressibility in tetragonal beam structures.” Mechanics of Materials 46 (2012): 123-128.
[72] Silverberg, Jesse L., et al. ”Using origami design principles to fold reprogrammable mechanical metamaterials.” science 345.6197 (2014): 647-650.
[73] Lakes, Roderic S., et al. ”Extreme damping in composite materials with negative-stiffness inclusions.” Nature 410.6828 (2001): 565-567.
[74] Lakes, Roderic S., et al. ”Extreme damping in composite materials with negative-stiffness inclusions.” Nature 410.6828 (2001): 565-567.
[75] Gao, Renjing, et al. ”A negative-stiffness based 1D metamaterial for bidirectional buffering and energy absorption with state recoverable characteristic.” Thin-Walled Structures 169 (2021): 108319.
[76] Zhu, Shaowei, et al. ”A novel bi-material negative stiffness metamaterial in sleeve-type via combining rigidity with softness.” Composite Structures 262 (2021): 113381.
[77] Chen, Shuai, et al. ”A novel gradient negative stiffness honeycomb for recoverable energy absorption.” Composites Part B: Engineering 215 (2021): 108745.
[78] Schenk, Mark, and Simon D. Guest. ”Geometry of Miura-folded metamaterials.” Proceedings of the National Academy of Sciences 110.9 (2013): 3276-3281.
[79] Wang, Y. C., and R. S. Lakes. ”Composites with inclusions of negative bulk modulus: extreme damping and negative Poisson’s ratio.” Journal of Composite Materials 39.18 (2005): 1645-1657.
[80] Meza, Lucas R., Satyajit Das, and Julia R. Greer. ”Strong, lightweight, and recoverable three-dimensional ceramic nanolattices.” Science 345.6202 (2014): 1322-1326.
[81] Jang, Dongchan, et al. ”Fabrication and deformation of three-dimensional hollow ceramic nanostructures.” Nature materials 12.10 (2013): 893-898.
[82] Zheng, Xiaoyu, et al. ”Ultralight, ultrastiff mechanical metamaterials.” Science 344.6190 (2014): 1373-1377.
[83] Yang, Chen, et al. ”4D printing reconfigurable, deployable and mechanically tunable metamaterials.” Materials Horizons 6.6 (2019): 1244-1250.
[84] Akbari, Saeed, et al. ”Enhanced multimaterial 4D printing with active hinges.” Smart Materials and Structures 27.6 (2018): 065027.
[85] Qi, Jixiang, et al. ”Recent progress in active mechanical metamaterials and construction principles.” Advanced Science 9.1 (2022): 2102662.
[86] Akbari, Saeed, et al. ”Multimaterial 3D printed soft actuators powered by shape memory alloy wires.” Sensors and Actuators A: Physical 290 (2019): 177-189.
[87] Zhao, Zeang, et al. ”Stiff reconfigurable polygons for smart connecters and deployable structures.” International Journal of Mechanical Sciences 161 (2019): 105052.
[88] Yuan, Chao, et al. ”3D printed reversible shape changing soft actuators assisted by liquid crystal elastomers.” Soft Matter 13.33 (2017): 5558-5568.
[89] Minori, Adriane F., et al. ”Reversible actuation for self-folding modular machines using liquid crystal elastomer.” Smart Materials and Structures 29.10 (2020): 105003.
[90] Nick, Zachary H., Christopher E. Tabor, and Ryan L. Harne. ”Liquid metal microchannels as digital sensors in mechanical metamaterials.” Extreme Mechanics Letters 40 (2020): 100871.
[91] Jolly, Mark R., J. David Carlson, and Beth C. Munoz. ”A model of the behaviour of magnetorheological materials.” Smart materials and structures 5.5 (1996): 607.
[92] Montgomery, S. Macrae, et al. ”Magneto-mechanical metamaterials with widely tunable mechanical properties and acoustic bandgaps.” Advanced Functional Materials 31.3 (2021): 2005319.
[93] Kim, Yoonho, et al. ”Printing ferromagnetic domains for untethered fast-transforming soft materials.” Nature 558.7709 (2018): 274-279.
[94] Novelino, Larissa S., et al. ”Untethered control of functional origami microrobots with distributed actuation.” Proceedings of the National Academy of Sciences 117.39 (2020): 24096-24101.
[95] Ma, Chunping, et al. ”Magnetic multimaterial printing for multimodal shape transformation with tunable properties and shiftable mechanical behaviors.” ACS Applied Materials & Interfaces 13.11 (2020): 12639-12648.
[96] Gu, Hongri, et al. ”Magnetic quadrupole assemblies with arbitrary shapes and magnetizations.” Science Robotics 4.35 (2019): eaax8977.
[97] Chen, Yuzhen, and Lihua Jin. ”Geometric role in designing pneumatically actuated pattern-transforming metamaterials.” Extreme Mechanics Letters 23 (2018): 55-66.
[98] Pan, Qi, et al. ”Programmable soft bending actuators with auxetic metamaterials.” Science China Technological Sciences 63.12 (2020): 2518-2526.
[99] Narang, Yashraj S., Joost J. Vlassak, and Robert D. Howe. ”Mechanically versatile soft machines through laminar jamming.” Advanced Functional Materials 28.17 (2018): 1707136.
[100] Tan, Xiaojun, et al. ”Real-time tunable negative stiffness mechanical metamaterial.” Extreme Mechanics Letters 41 (2020): 100990.
[101] Haghpanah, Babak, et al. ”Programmable elastic metamaterials.” Advanced Engineering Materials 18.4 (2016): 643-649.
[102] D.Thomas. ”Active metamaterials: unit cells for tunable damping”. Delft University of Technology, Delft (2020).
[103] N.S.Saravana Jothi and A. Hunt. ”Active mechanical metamaterial with embedded piezoelectric actuation”. Delft University of Technology, Delft (2022).
[104] Chen, Tian, Mark Pauly, and Pedro M. Reis. ”A reprogrammable mechanical metamaterial with stable memory.” Nature 589.7842 (2021): 386-390.
[105] Poon, Ryan, and Jonathan B. Hopkins. ”Phase-Changing Metamaterial Capable of Variable Stiffness and Shape Morphing.” Advanced Engineering Materials 21.12 (2019): 1900802.
[106] Tan, Xiaojun, et al. ”Design, fabrication, and characterization of multistable mechanical metamaterials for trapping energy.” Extreme Mechanics Letters 28 (2019): 8-21.
[107] Overvelde, Johannes TB, et al. ”A three-dimensional actuated origami-inspired transformable metamaterial with multiple degrees of freedom.” Nature communications 7.1 (2016): 1-8.
[108] Wei, Yu-Ling, et al. ”Design and analysis of 2D/3D negative hydration expansion Metamaterial driven by hydrogel.” Materials & Design 196 (2020): 109084.
[109] Liu, Jia, et al. ”Harnessing buckling to design architected materials that exhibit effective negative swelling.” Advanced Materials 28.31 (2016): 6619-6624.

# 3

# Thesis report - Magnetorheological fluid damper for tunable damping in active mechanical metamaterials

# Magnetorheological fluid damper for tunable damping in active mechanical metamaterial

Samer Habbal

*dept. Precision and Microsystems Engineering*
*Delft university of technology*
Melkweg 2, 2628CD, Delft, the Netherlands
s.habbal@tudelft.nl

***Abstract*—In the era of advancing technology, the demand for specialized engineering materials has risen significantly. Active Mechanical Metamaterials (AMMs) offer a novel approach to engineering materials with tunable mechanical properties. This research focuses on developing tunable damping active mechanical metamaterials (AMMs) by incorporating magnetorheological fluid (MRF) damper into a compliant mechanism unit cell. This unit cell transforms linear displacement into rotation at the centre, precisely where the damper is located. First, The AMM unit cell has been designed with a compliant structure that converts the unit input into an embedded MRF damper. After that, the dynamic behaviour of the unit cell was studied by combining analytical and FEM modelling to characterize the stiffness and damping of the unit cell. A prototype has been built, and the damping and stiffness have also been experimentally characterized. The results highlight key findings, including numerical data, offering insights into the efficiency of the unit cell's compliant transformation mechanism and the tunable damping achieved through MRF dampers, where the damping ratio can be adjusted from 0.02 to approximately 0.03 when 1.4 A of current is applied. This study represents a significant advancement in active mechanical metamaterials, showcasing a novel unit cell design where the magnetorheological fluid has been used for the first time to achieve tunable damping in active mechanical metamaterials. The success of this study is evident in the convergence of theoretical predictions with experimental outcomes, emphasizing the robustness of the proposed design and modelling methodologies. The implications of this research extend to diverse applications in structural engineering and vibration control, with a particular focus on high-tech systems. These findings provide valuable guidance for researchers and engineers working in high-tech industries, offering practical insights that can significantly impact the development and implementation of innovative solutions in these fields.**

***Index Terms*—Smart materials, Magnetorheological, Complaint mechanism, Damping, Finite-element analysis, Vibration test.**

## I. Introduction

As technology advances, the demand for specialized engineering materials to meet the innovation requirements of various application fields such as medicine, aerospace, automotive, and many others has significantly increased [2]. These materials are crucial in bringing new products and technologies to the market to enhance human life and improve efficiency in various industries. Mechanical metamaterials (MMs) have unique mechanical properties based on their structures instead of conventional components [4], [5]. These materials have emerged in recent years thanks to the advancements in additive manufacturing technologies and the widespread availability of 3D printers. These tools have enabled the production of materials with highly complex micro/nanoarchitecture. MMs typically consist of a lattice structure (cellular materials), with unit cells assembled to fill the material space. The intricate behaviours of these metamaterials can be achieved by manipulating the shape, geometry, orientation, and arrangement of unit elements [1].

While MMs offer a wide range of properties beyond traditional materials, these characteristics are inherently fixed by the initial design. However, the recent development of Active Mechanical Metamaterials (AMM) marks an evolutionary change. By incorporating sensors and actuators within the unit elements, AMMs provide centralized and localized control over the distribution of material properties and states within the lattice [1]. This innovative approach imbues mechanical metamaterials with a dynamic and adaptive nature, enabling tunable and responsive material properties.

The development of AMMs is still in its early stages, and the current state of the art is limited. Previous research has explored various stimuli, such as thermal and pneumatic actuation [9], to achieve AMM properties, but these approaches often experience long response times. Some researchers have turned to smart material actuators to pursue real-time active control over AMM properties [10]. One noteworthy advancement was presented by Haghpanah et al [7]. They created a programmable elastic AMM by integrating mechanical metamaterial lattices with electromagnets. The electromagnets effectively lock the struts of the unit cell when switched on, enabling individual control over unit cell stiffness and, consequently, adjustment of the lattice's elastic properties [7]. Jothi and Hunt proposed a concept for achieving dynamic control over material configuration and dynamic state by embedding commercially available piezoelectric stack actuators within AMMs [1]. Further exploration of this approach holds the potential to realize dynamic

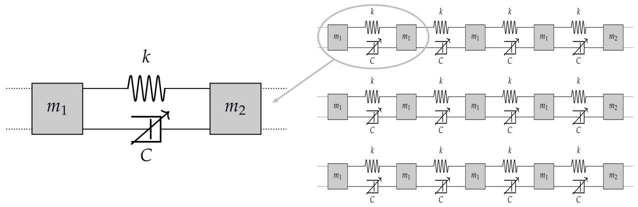


Figure 1: Conceptual representation of active mechanical metamaterial lattice

control over stress or strain fields within the material. Thomas and Hunt took a different route, developing an active unit cell with embedded miniaturized electromagnet actuators designed to achieve active damping through electromagnetic alteration of Coulomb friction [8]. However, this structure lacks dynamic control as the actuators cannot forcibly manipulate the structure. Ongoing research seeks to overcome these limitations and unlock the full potential of dynamically controlled AMMs.

The primary objective of this project is to realize active mechanical metamaterials featuring tunable damping, precisely eliminating Coulomb damping (friction). Integrating magnetorheological fluid dampers, also known as MRF dampers, within active mechanical materials (AMMs) marks a significant innovation in material science and engineering. This invention overcomes the drawbacks of coulomb damping. By embedding MRF dampers within AMMs, we introduce a dynamic and tunable element to the material, allowing for real-time adjustments of its mechanical characteristics. MRFs are specialized smart fluids containing magnetically responsive particles suspended within a liquid carrier [11]. MRF dampers have many advantages, including contactless and silent fluid control without moving parts, a sizeable controllable range and force capacity, quick response times, and low power requirements [13].

This thesis report explores the design and performance of a tunable damping Active Mechanical Metamaterial (AMM) unit cell. It is divided into several sections, each contributing to a complete understanding of the developed tunable damping AMM unit cell. First, the specific MRF damper and the respective AMM unit cell are designed, as explained in Section (II-A). Thereafter, the magnetorheological fluid is characterized in Section (II-B), which is followed by modelling in Section (II-C), where a combination of analytical working and FEM analysis has been executed to model the dynamic behaviour of the unit cell and subsequently identifying the stiffness and damping ratio of the unit cell. The Section on experimental evaluations (II-D) includes the prototyping of the AMM unit cell and the measurement of its performance. The subsequent Results (Section III) present findings related to MRF characterization, compliant transformation mechanism performance, the stiffness of the unit cell, magnetic circuit, simulated and experimentally estimated dynamic responses, and damping ratio of the AMM unit cell. Thereafter, the discussion (Section IV) interprets the results, providing insights into the research implications. Finally, the conclusion (Section V) summarizes the essential findings and their significance.

## II. Methodology

The process is divided into four main phases, which are depicted in the flowchart shown in Figure 2. These phases include design, MRF experimental characterization, modelling, and experimental evaluation. Each step is crucial for gaining insights into the performance and behaviour of the proposed AMM unit cell. The flowchart in Figure 2 demonstrates that the stiffness and damping ratio of the unit cell have been determined through experimental characterization and modelling.

### A. The design of AMM unit cell

*1) Structural design of the unit cell:* The initial concept involved utilising MRF dampers to achieve adjustable viscous damping. The unit cell of the proposed tunable damping AMM requires (1) the need for compact dimensions, emphasizing the importance of minimizing size and ensuring the potential for miniaturization, (2) mechanical structure that provides the lattice stiffness, converts the material deformation into sufficient input on the MRF damping element and accommodates that damping element. These requirements collectively shape the structural and functional aspects of the AMM unit cell.

The design of the AMM unit cell draws inspiration from the spring-mass (damper) modelling of material structures. In this conceptualization, the material is perceived as a network of nodes, each possessing mass. Nodes are interconnected by vertices characterized by stiffness and damping, as shown in Figure 1. The properties of these structures can be adjusted by manipulating or introducing an actuator between two nodes, providing a dynamic means of controlling the material's mechanical behaviour.

Several designs based on traditional MRF damper configurations were considered, but they were dismissed due to limitations in miniaturization, a crucial requirement for the procedure. To overcome this limitation, a novel concept emerged involving two parallel plates with magnetorheological fluid between them, as shown in Figure 3. Where the rectangular parts 'A' form the nodes of the unit cell and the external vertices(leaf springs) 'B' serve the stiffness of the unit cell. The two disks in the middle of the unit cell form the bases where the damper will be built. These disks contribute to a mechanical transformation mechanism, converting linear movements between two nodes into rotational

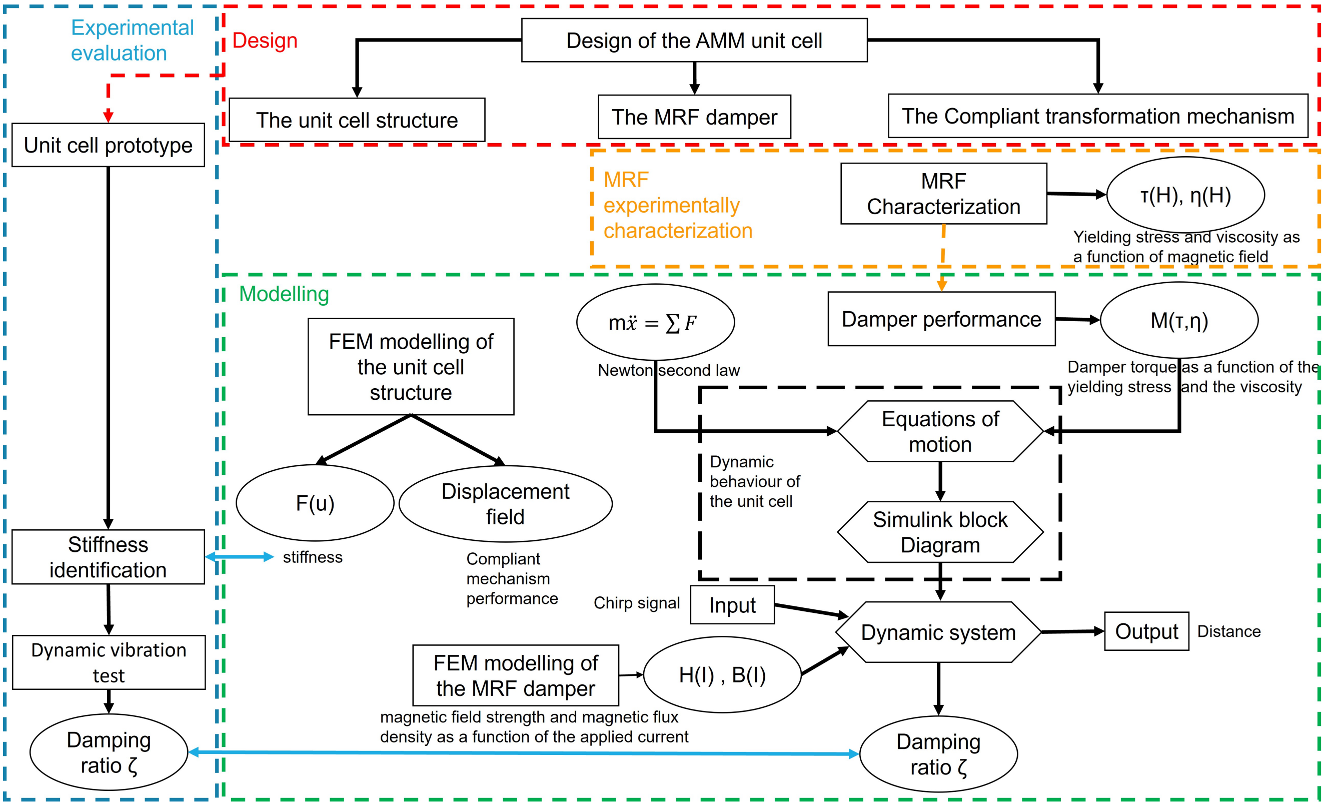


Figure 2: Methodology flowchart illustrating the step-by-step process followed in this research

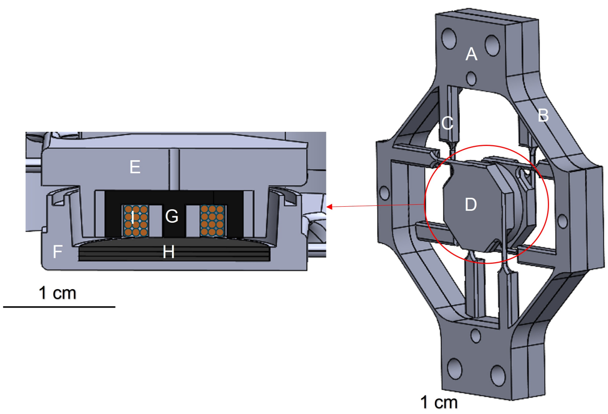


Figure 3: Design elements of the Active Mechanical Metamaterial (AMM) unit cell: A) Node B) Leaf spring C) Compliant transformation mechanism D) Magnetorheological Fluid (MRF) damper E) Damper upper disk F) Damper lower disk G-H) Magnetic core (ferrite) I) Coil

movements. This rotational movement, influenced by the MRF, effectively controls the damping characteristics within the material, offering a dynamic and responsive mechanism.

*2) The design of the complaint transformation mechanism:* The design is based on compliant mechanisms because of miniaturization needs and the elimination of Coulomb friction. Unfortunately, the existing literature does not offer a suitable mechanism. Consequently, an innovative, compliant design has been developed to convert linear to rotational motion.

Figure 3 displays this compliant mechanism, which comprises four compliant hinges, 'C', that link the unit cell nodes with the rotational disk located at the centre of the unit cell. These hinges restrict the disk's movement to rotational motion, fulfilling the specific requirements of the active mechanical metamaterial (AMM) unit cell. Additionally, to enable rotation in opposite directions of the two parallel disks, the unit cell has two layers that show 90 degrees of symmetry rotation of the four hinges.

This innovative approach not only fulfils the intricate requirements of the transformation process but also contributes to the overall adaptability and responsiveness of the AMM unit cell's mechanical behaviour.

*3) The design of the magnetorheological damper:* The integral component of the Active Mechanical Metamaterial (AMM) unit cell is the magnetorheological (MR) damper, designed to provide tunable damping through innovative mechanisms. This damper's design involves features that manipulate the rheological properties of magnetorheological fluid, thereby controlling the damping force exerted within the unit cell.

The MRF damper comprises two rotating disks (Figure 3 E, F) with a gap housing the magnetorheological fluid. The magnetorheological fluid responds dynamically to changes in the magnetic field. The rheological properties of this fluid can be fine-tuned by applying a magnetic field, altering its viscosity, and yielding shear stress. This dynamic adjustability enables rapid and precise control over the unit cell's response. A dedicated magnetic circuit is integrated into the damper design to facilitate the modulation of magnetic fields. This circuit comprises a coil (Figure 3 I) wound around an E-core (Figure 3 G) strategically positioned within the upper disk. Additionally, the lower disk incorporates an iron component (Figure 3 H). The E-core design enhances the magnetic properties of the upper disk, contributing to the efficient generation and manipulation of the magnetic field in the gap between the rotating disks.

### *B. Rheological characterization of MRF fluid*

Magnetorheological Fluids (MRFs) exhibit a remarkable transition from a liquid to a semisolid state, characterized by limited fluid movement, within a few milliseconds when exposed to a magnetic field [12].

To study the damping performance of MR fluid, it is necessary to experimentally characterize it first. This will help in understanding the complex relationship between the applied magnetic field strength and the yielding stress, which is crucial for analytical study or modelling. In this section, we characterized the commercially available MRHCCS4-A MRF, employing the advanced capabilities of the Anton Paar rheometer (MCR 301e).

A series of experiments were conducted to characterize the rheological properties of MRHCCS4-A MRF at different applied currents from $0A$ to $1.5A$. All experiments were performed under a constant temperature of 20°C. A flow curve test was executed, systematically sweeping the shear rate from $0(1/s)$ to $100(1/s)$ A and measuring the corresponding shear stress. These experiments, complemented by Bingham model analysis integrated into the Anton Paar software, allowed for determining the yield stress at different magnetic field strengths, a fundamental parameter for understanding the MRF's behaviour across diverse magnetic field strengths. These data was used to perform comprehensive curve fitting. The resulting fitted curve established a mathematical relationship between yield stress and magnetic field strength.

### *C. Modelling*

This modelling aims to analyse the performance of the unit cell at different actuation currents. The process can be shown step by step in the green modelling part of Figure 2. Firstly, in Subsection II-C1, the damping performance of the embedded damper has been analyzed

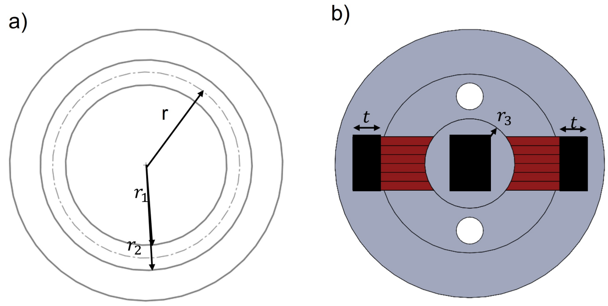


Figure 4: Systematic of the functional area of the embedded damper

analytically, by calculating the damping torque as a function of the yielding stress and viscosity exhibited by the embedded MRF damper. In the following sections, the dynamic behaviour of the unit cell is analyzed. Firstly, in Subsection II-C2, the equations of motion are used to describe the unit cell's behaviour. Secondly, Subsection II-C3 characterizes the magnetic circuit with the help of FEM Analysis. This analysis results in the magnetic field strength as a function of the applied current. Thirdly, in Subsection II-C4, Simulink is used to simulate the dynamic behaviour of the unit cell. This simulation results in the transformation function of the unit cell at different applied currents, which is then used to execute the damping ratio. In addition, another FEM modelling is executed in Subsection II-C5 to describe the performance of the compliant transformation mechanism and identify the stiffness of the unit cell.

*1) The Damping performance of the embedded MRF damper:* To analyze the damping performance of the embedded MRF damper, The functional area shown in figure 4 is conceptually treated as a ring characterized by radii $r_1$ and $r_2$. This analysis uses the Bingham model to describe the rheological properties of the MRF fluid.

The total damping torque ($M$) is a combination of the MRF-magnetic shear-yielding ($M_H$) and the viscous torque ($M_\eta$) generated by the MRF viscosity. MR fluids behave in a non-Newtonian manner in the presence of a magnetic field; that is, the strain of the fluid is non-linearly correlated with the stress [3]. Utilizing the Bingham model for the MRF fluid, the shear stress ($\tau$) is expressed as:

$$\tau = \tau_y(H) + \eta\dot{\gamma}$$

Here, $\tau_y(H)$ represents the yield stress influenced by the applied magnetic field ($H$), and $\eta$ denotes the viscosity of the MRF fluid. The $\dot{\gamma}$ signifies the shear rate. The subsequent equations capture the essence of the Bingham model, providing a foundation for assessing the MRF damper's torque within the specified working area.

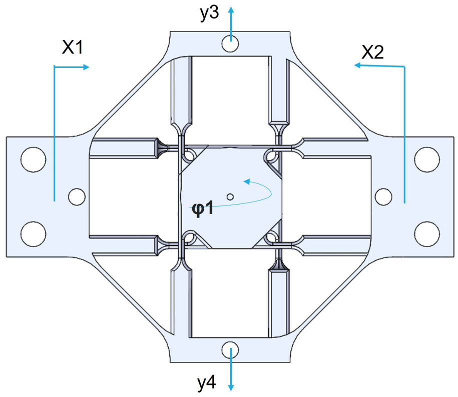


Figure 5: The linear displacements of the unit cell nodes and the angular displacement of the damper disk

$$M = M_H + M\eta$$

$$M_H = \int_{r_1}^{r_2} 2\pi r^2 \tau_y \, dr$$

$$M_H = \frac{2\pi}{3} \tau_y (r_2^3 - r_1^3)$$

$$M_\eta = \int_{r_1}^{r2} 2\pi r^3 \eta \frac{2\omega r}{h} \, dr$$

$$M_\eta = \frac{\pi \omega_1 \eta}{h} (r_2^4 - r_1^4)$$

$$M = \frac{2\pi}{3} \tau_y (H)({r_2}^3 - {r_1}^3) + \frac{\pi \omega_1 \eta}{h} ({r_2}^4 - {r_1}^4)$$

Considering the damper's structure, which includes a part of the calculated ring with thickness $t$ and a circular area in the middle, the torque equation is further refined:

$$M = A_1 \omega_1 \eta(H) + A_2 \tau_y(H) sgn(\omega_1) \quad (1)$$

Here, $A_1$ and $A_2$ are constants that encapsulate the dimensions of the damper:

$$A_1 = \frac{2t(r_2^4 - r_1^4)}{h(r_1 + r_2)} + \frac{\pi r_3^4}{h} \qquad A_2 = \frac{4t(r_2^3 - r_1^3)}{3(r_1 + r_2)} + \frac{2\pi}{3} r_3^3$$

*2) The dynamic behaviour of the unit cell:* This subsection explores the dynamic behaviour of the AMM unit cell, focusing on constraint equations and equations of motion. The unit cell's design aims to transform linear displacements into a pure rotation of the damper located at the centre of the unit cell. Mathematical representations of these constraints and the motion equations provide a complete understanding of the unit cell's dynamic response.

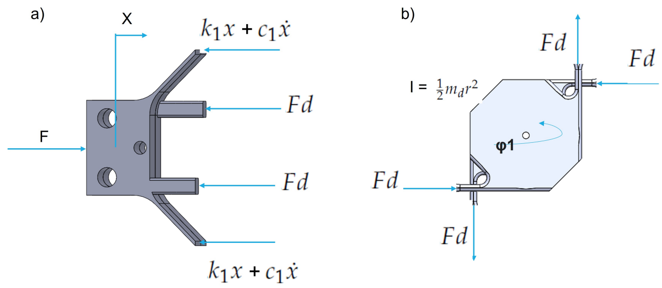


Figure 6: Free body diagram of a) left node b) upper disk

- constraint equations: The unit cell's constraints, essential for achieving the desired mechanical behaviour, are expressed through mathematical equations:
  1) The displacements in the four nodes of the unit cell are equal, as shown in figure 5.

$$x_1 = -x_2 = y_3 = -y_4 \quad (2)$$

  2) The two rotating disks have identical angular displacements directed in opposite directions. For small displacements, these displacements can be described as follows:

$$\varphi_1 = \frac{x}{r} = -\varphi_2 \quad (3)$$

- The equations of motion: The equations of motion, fundamental for analyzing the unit cell's dynamic response, are derived based on the displacement and rotation constraints.
  The equation of motion for the left mass is derived using the free body diagram shown in Figure 6a.

$$m_1 \ddot{x} - 2k_1 x - 2c_1 \dot{x} - 2F_d = F$$

Here, $k_1$ and $c_1$ represent the stiffness and damping coefficient of the leaf springs, and $F_d$ is the force associated with the compliant transmission mechanism.
The equation of motion for the rotating upper disk is derived using the free body diagram shown in Figure 6b.

$$4F_d r = I \ddot{\varphi}_1 + M_d$$

This equation encapsulates the rotational dynamics of the damper upper disk, considering the angular displacement of the upper disk $\varphi_1$, the damping torque ($M_d$), inertia ($I$), which equals to $\frac{1}{2} m_d r^2$, and the force associated with the compliant transmission mechanism ($F_d$)
By employing the constraint equations (2, 3), the force $F_d$ can be expressed as:

$$F_d = \frac{1}{16} [m_d \ddot{x} + \frac{M_d}{4r}]$$

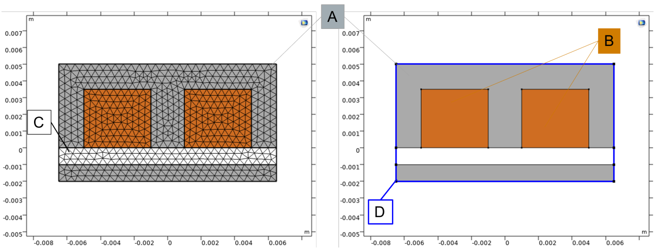


Figure 7: Comsol finite element modelling of the magnetic circuit. Different domains of the model are depicted: A represents the iron core, B represents the coil, C illustrates the gap with Magnetorheological Fluid (MRF), and D shows the magnetic insulations.

This equation is added to the equations of motion, yielding a more sophisticated formulation that considers the impacts of the compliant transformation mechanism on the unit cell's overall dynamic response.

$$(m + \frac{1}{8}m_d)\ddot{x} = F - 2K_1 x - 2C_1\dot{x} - \frac{M_d}{2r}$$

Incorporating the damping torque into this equation, the equation of motion (Equation 4) is obtained.

$$(m + \frac{1}{8}m_d)\ddot{x} = F - 2K_1 x - 2C_1\dot{x} - \frac{A_1}{4r^2}\eta(H)\dot{x} - \frac{A2}{2r}\tau_y(H)sgn(\dot{x}) \quad (4)$$

*3) Finite element modelling of the magnetic circuit:* Finite Element Modeling (FEM) was used to examine the magnetic circuit of the MRF damper. Figure 7 depicts the research, which underlined three critical domains: the iron core, the coil, and the gap. The iron core, vital in directing magnetic flux, was modelled to evaluate its impact on the damper's efficiency. By simulating the coil's behaviour under different conditions, we better understood its function in generating a magnetic field. The third domain, the gap, incorporates MRF, and a cutline was introduced in the gap to visualize magnetic field and flux changes over the gap. This FEM analysis provides valuable insights into the MRF damper's magnetic characteristics, which aid in understanding its operation and potential applications.

*4) Dynamic modelling of the Unit Cell using Simulink:* Dynamic modelling is crucial to understanding how the proposed AMM unit cell responds to varying conditions. Using Simulink, a simulation can be conducted to observe and analyze the AMM unit cell's dynamic response when the actuation input is varied. The dynamics of the unit cell, encapsulated in equation 4, are translated into a Simulink block diagram, as illustrated in Figure 8. This model allows for simulating the response of the unit cell

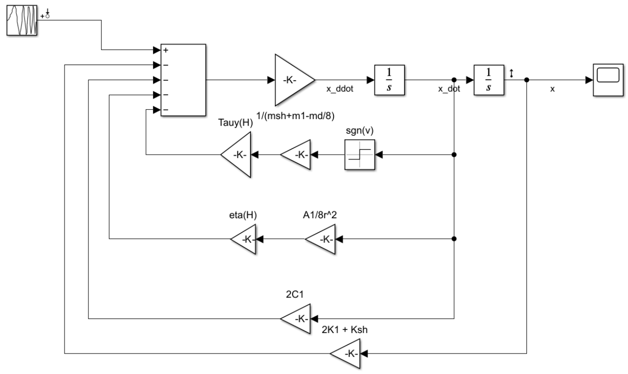


Figure 8: Simulink block diagram of the dynamic of the unit cell

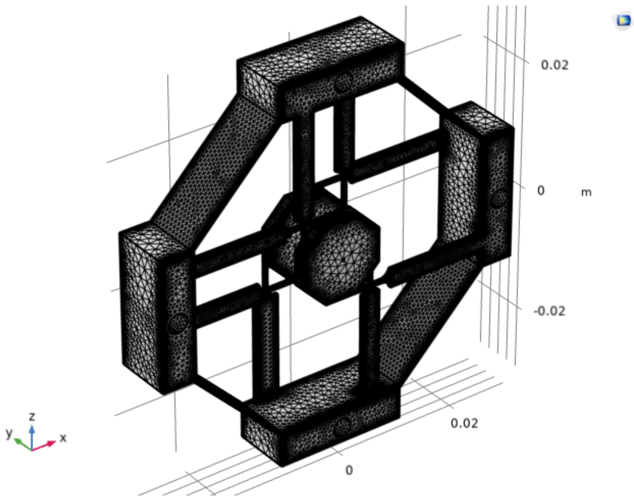


Figure 9: Comsol finite element modelling of the compliant unit cell structure

across varying magnetic flux densities, thereby exploring its dynamic behaviour. By employing a chirp signal as the input and monitoring the output displacement, the simulation facilitates the characterization of the unit cell's dynamic response through linear analysis. This dynamic modelling approach contributes significantly to understanding the AMM unit cell's complex behaviour. Consequently based on the transfer function of the modelled system the damping ratio can be determined using the MATLAB function 'damp'.

*5) Finite element modelling of the compliant structure of the unit cell:* Finite Element Modeling (FEM), as shown in Figure 9, was performed in Comsol Multiphysics 6.0 to study the compliant transformation mechanism used to convert linear displacement to pure rotation and to analyze the overall stiffness of the designed unit cell structure. The deformation field of the AMM unit cell was examined for various displacement inputs up to $5mm$ displacement of each mass (node). Two probe nodes were chosen in the middle of the rotating disks

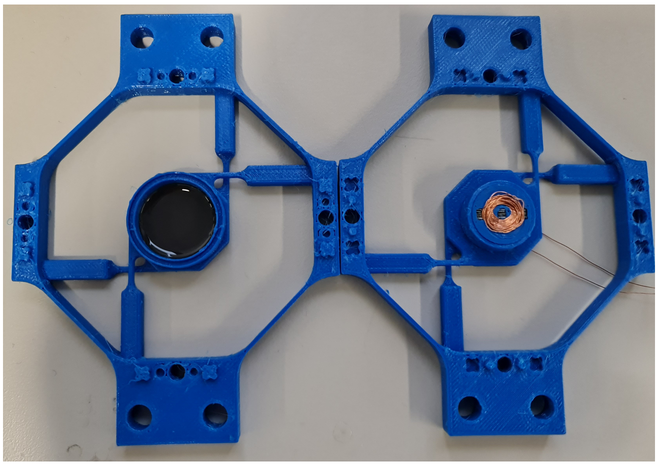

Figure 10: A prototype of the AMM unit cell with an integrated MRF damper

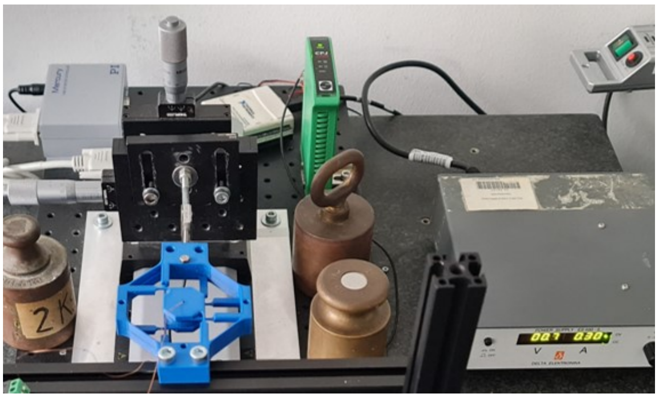

Figure 11: PI stage tensile test for complaint mechanisms

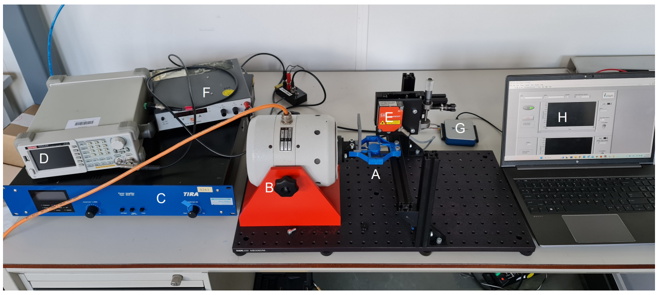


Figure 12: Vibration test setup A) unit cell B) vibration shaker C) Amplifier D) signal generator E) Laser distance sensor F) Power supply G) acquisition board H) PC with NI LabVIEW 2018 environment

for the first purpose. Displacement was applied to the upper and lower masses, and the displacement of the centre of the disks was studied to ensure pure rotational movements of the damper disks. The simulation was conducted for a sweep of displacements up to $5mm$ to generate an animation of the displacement field of the mechanism. For the second purpose, namely calculating the stiffness of the unit cell, a force-displacement curve was generated for a probe point of the upper mass (node) with the lower one fixed.

### *D. Experimental evaluation*

The experimental evaluation phase is crucial in validating the design and assessing the performance of the AMM unit cell. The AMM unit cell prototype was first constructed as explained in Subsection II-D1. Two distinct experiments were conducted to validate and understand the behaviour of the proposed unit cell. The first experiment in Subsection II-D2 focused on the structural stiffness of the compliant mechanism, while the second experiment in Subsection II-D3 aimed to characterize the damping properties of the unit cell by conducting a dynamic vibration test.

*1) AMM unit cell prototype:* The AMM unit cell was manufactured using Polyethylene Terephthalate modified with Glycol (PETG) on a Prusa i3 MK3s+ 3D printer. This approach facilitated the creation of the entire structure in two parts, easily assembled through integrated click-in mechanisms at the nodes.

The damper is composed of several components, including the PETG-printed holder, the iron core crafted from layers of 0.5 mm magnetic steel cut to the desired form using laser cutting techniques, and the coil consisting of 150 turns of 0.2 mm enamelled copper wire, wound using an automated coil winder. Figure 10 displays an assembled AMM unit cell, showcasing the successful integration of these components into a functional prototype.

*2) Stiffness identification experimentally:* The experiment was conducted utilizing a PI stage tensile test, where force-displacement measurements were taken at various levels of actuation current, as shown in Figure 11. This experimental setup allowed for determining the stiffness of the compliant structure within the unit cell. The test was conducted multiple times using varying levels of actuation current ($0$ *to* $1$ $A$) to ensure that the damper did not impact the stiffness of the unit cell. The results obtained from this test offer valuable insights into the static behaviour and structural integrity of the AMM unit cell.

*3) Dynamic vibration test:* The dynamic vibration test setup, illustrated in Figure 12, comprises essential components such as a vibration shaker, a displacement laser sensor, and associated equipment. In this configuration, the displacement serves as the output, while the input is the voltage supplied to the shaker.

The voltage input is generated using a signal generator (Figure 12-D), which drives the shaker through an amplifier (Figure 12-C). Specifically, a chirp signal with a frequency sweep ranging from 0.1 to 200 Hz, a sweeping time of 50 seconds, and three repetitions is employed

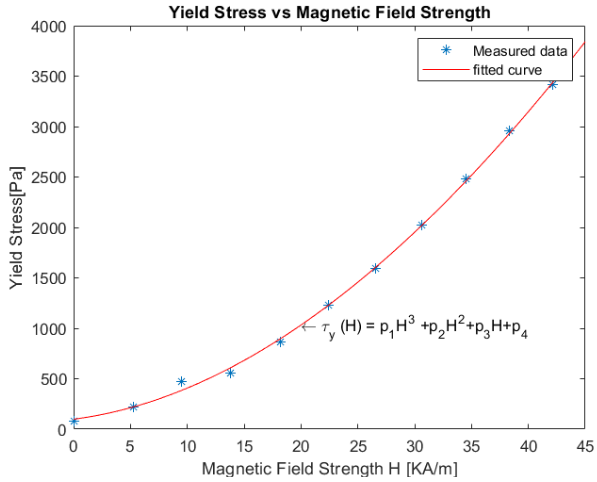


Figure 13: Yield stress as a function of the magnetic field strength of MRHCCS4-A

as the input. The displacement output is measured by a laser distance sensor (Figure 12-E), and the acquired data is digitally processed using an acquisition board interfaced with the NI LabVIEW 2018 environment on a PC (Figure 12-H).

The dynamic vibration test is executed with varying applied currents, ranging from 0 $A$ to 1.4 $A$. To mitigate the impact of heating, the unit cell is allowed to cool to room temperature after each test iteration. The transfer function of the unit cell is estimated using the measured data, employing the Matlab function 'tfestimate'. Before testing the unit cell, a preliminary dynamic assessment of the shaker is conducted to comprehend its dynamic behaviour.

Analyzing the transfer function provides valuable insights into the damping characteristics of the unit cell. This dynamic evaluation facilitates understanding the unit cell's responsiveness and tunable damping features. The damping ratio ($\zeta$) is calculated from the Q factor of the resonance peak, utilizing the formula

$$\zeta = \frac{1}{2Q}$$

Analyzing the transfer function provides useful information about the damping characteristics of the unit cell. This assessment helps to understand the unit cell's responsiveness and tunable damping features.

## III. Results

This section outlines the outcomes derived from both the modeling and experimental assessments.

*1) Rheological characterization of the MR Fluid:* The MR Fluid has been experimentally characterized as detailed in Section II-B. The acquired dataset, including essential yield stress values, was used to perform curve fitting. The resulting fitted curve established a mathematical correlation between yield stress and magnetic field strength, which is dedicated to equation 5 and illustrated in Figure 13.

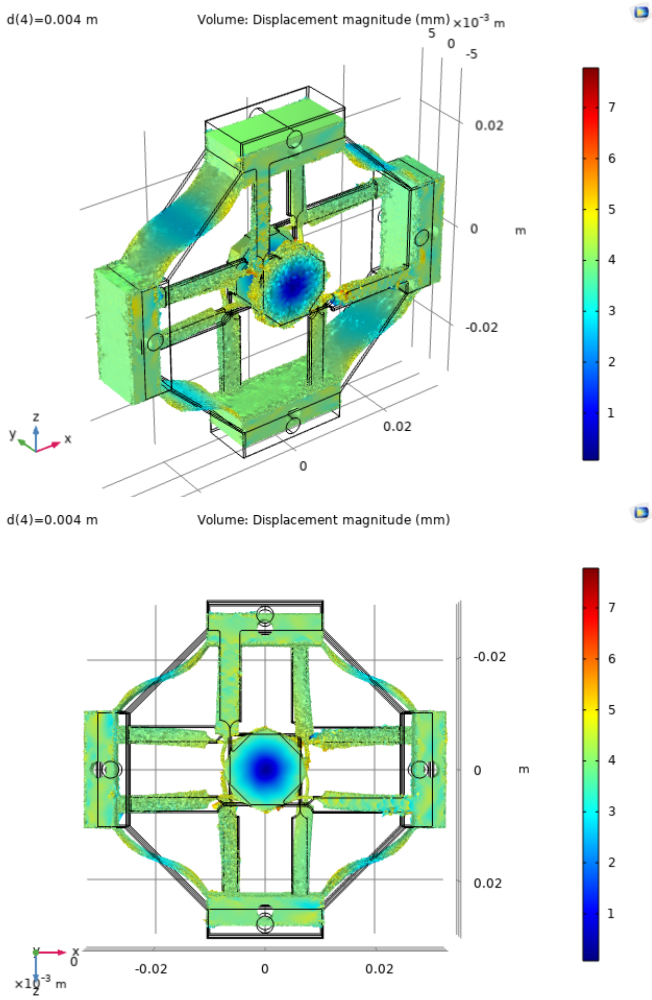


Figure 14: Displacement magnitude of the AMM unit cell

$$\tau_y(H) = -0.003493H^3 + 1.686H^2 + 14.36H + 98.91 \quad (5)$$

*2) Compliant Transformation Mechanism:* A Finite Element Modeling (FEM) analysis was performed to investigate the performance of the compliant transformation mechanism, as outlined in Subsection II-C5. Figure 14 illustrates the deformation field resulting from a 4 mm input displacement for each mass (node). The modelling results for all inputs indicate that the displacement of the centre of the rotating damper disks is negligible. The maximum displacement of the disk's centre is 150$\mu m$, with a relative displacement of the upper and lower disks of the damper reaching a maximum of 10$\mu m$.

*3) The stiffness of the unit cell:* The determination of the stiffness of the developed AMM unit cell involves both FEM analysis, discussed in Subsection II-C5, and experimental analysis, detailed in Subsection II-D2. In

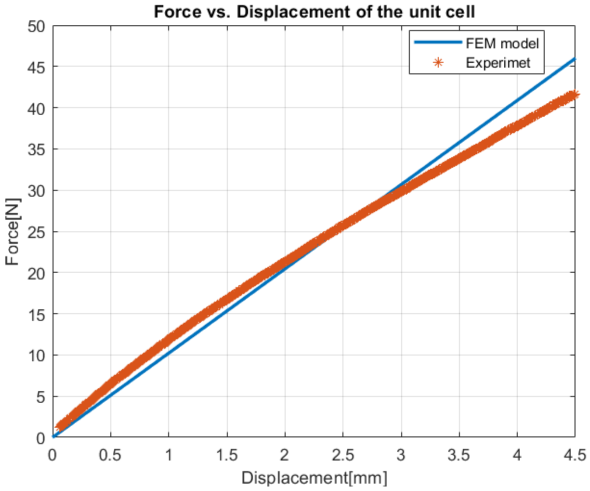


Figure 15: Force displacement diagram

Figure 15, the force-displacement diagram provides a comparative view of the modelled and experimental results. The slope of the force-displacement graph represents the stiffness of the AMM unit cell required for the dynamic analysis, measured at 1.022 kN/m.

*4) Magnetic circuit:* The FEM modelling results for the magnetic circuit, as discussed in Subsection II-C3, are presented in Figures 16a and 16b. Figure 16a illustrates the magnetic flux density in the magnetic circuit. Notably, Figure 16a reveals a loss of magnetization at the sharp corner of the magnetic core, emphasizing the need for further research to explore filleting options that could mitigate such losses. Figure 16b illustrates variations in the magnetic flux density across the damper gap. At 1.4 applied current, the magnetic flux density increases to 0.28 T in the ring working area, reaching 0.37 T in the circular working area in the centre of the gap. This provides crucial insights into the functional region of the damper.

*5) simulated dynamic of the unit cell:* The simulated dynamic behaviour of the AMM unit cell is investigated by employing a dynamic model developed in Simulink, as detailed in Section II-C4. The results, depicted in Figure 17, provide an insight into the unit cell's response under varying magnetic flux densities. Figure 17a presents the transmissibility of the AMM unit cell at various actuation current levels. Moreover, Figure 17b, which focuses on the peak area of the Bode plot diagram, shows a noticeable decrease in resonance peak amplitude as the applied current increases. Specifically, the amplitude of the resonance peak decreases from $-56dB$ to $-59dB$ at an applied current of 1.4 A, indicating an increase in damping and demonstrating the tunable and controllable nature of the AMM unit cell.

*6) Experimentally estimated dynamic of the unit cell:* The experimentally estimated dynamic behaviour of the AMM unit cell was thoroughly investigated by conducting experiments as detailed in Section II-D3. In Figure 18a, the transmissibility of the AMM unit cell, including the vibration shaker, is presented through a Bode plot diagram, revealing the system's behaviour at various actuation current levels. Figure 18b, focusing on the peak area of the Bode plot diagram, indicates a noticeable reduction in resonance peak amplitude with increasing applied current. Specifically, the amplitude of the resonance peak decreases from $-56.1dB$ to $-60.5dB$ at an applied current of 1.4 A.

*7) Damping ratio of the AMM unit cell:* The damping ratio was calculated by analyzing the modelled and experimentally estimated dynamic systems. After plotting both sets of results against the applied current, it was observed that there was a close resemblance between them, as shown in Figure 19. The damping ratio was tunable and varied from 0.02 when no current was applied to around 0.03 when 1.4 A of current was applied.

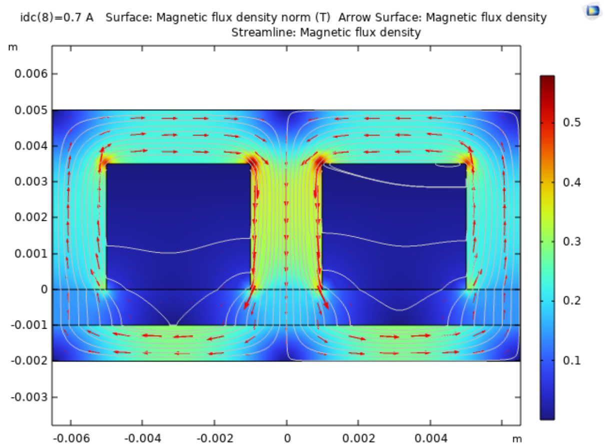


(a) The magnetic flux density of the magnetic circuit

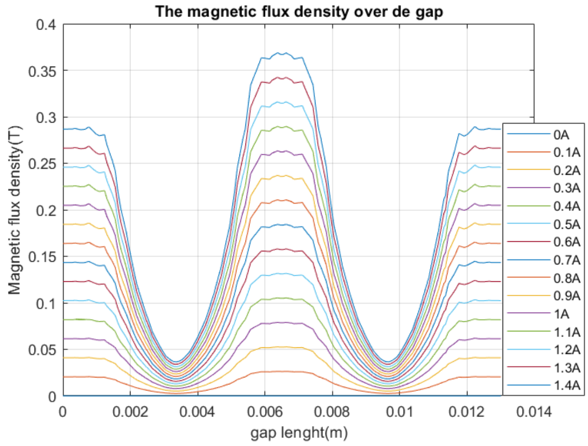


(b) The magnetic flux density over the gap

Figure 16: The results of magnetic circuit analysis through Comsol FEM

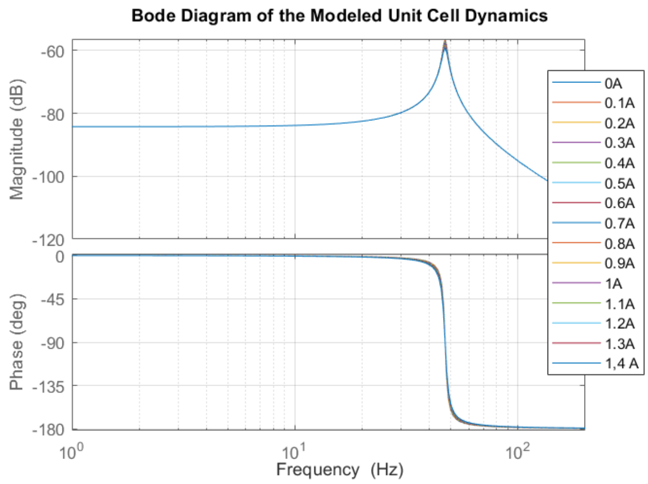


(a) Bode plot diagram of the modelled system of the AMM unit cell

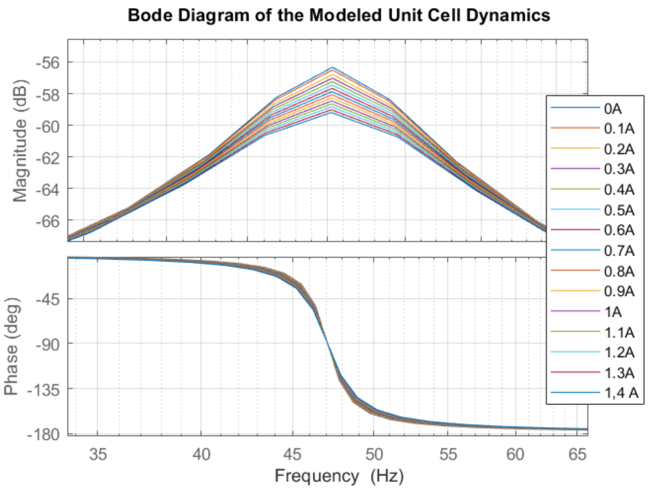


(b) Zooming in the peak area of the Bode plot diagram

Figure 17: Bode plot diagram of the modelled system of the AMM unit cell at different applied currents with a focus on the peak area.

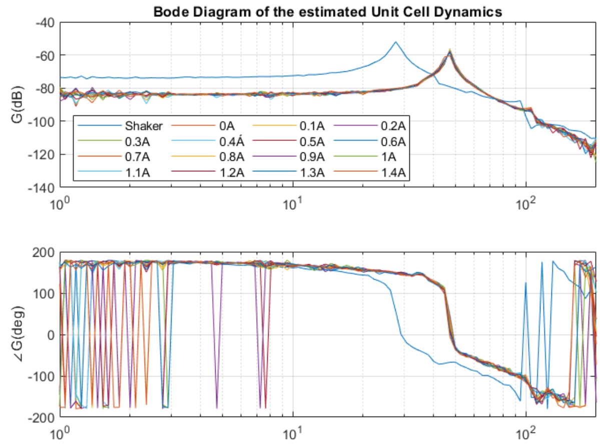


(a) Bode plot diagram of the experimentally estimated system of the AMM unit cell

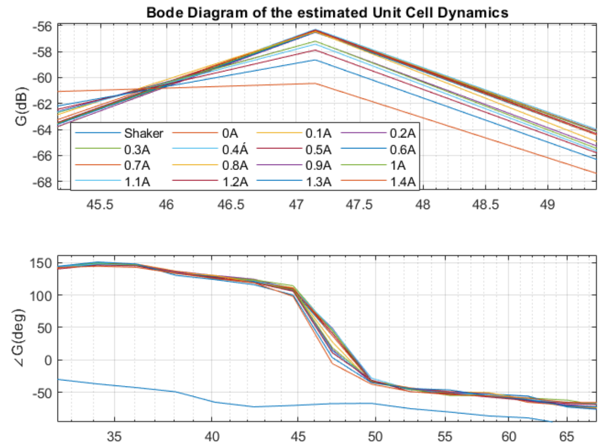


(b) Zooming in the peak area of the Bode plot diagram

Figure 18: Bode plot diagram of the experimentally estimated system of the AMM unit cell at different applied currents with a focus on the peak area

## IV. Discussion

This study presents a novel concept in active mechanical metamaterials (AMMs), focusing on a precisely engineered unit cell that enables tunable damping in dynamic systems. The key innovation lies in a sophisticated, compliant mechanism that transforms linear displacement into precise rotational movements, forming the basis for an integrated damper. The detailed FEM analysis emphasizes the efficiency of this transformation mechanism. Analyzing the displacement characteristics, it is evident that the damper disk in the centre of the unit cell experiences negligible displacement. These findings underscore the efficiency of the transformation mechanism, which imparts a pure rotation in the damper.

The comparison of the unit cell stiffness values, shown in Subsection III-3 obtained through both Finite Element Modeling (FEM) and experimental analysis, detailed in Subsection II-C5 and Subsection II-D2, serves as a critical validation step. The force-displacement diagram in Figure 15 illustrates the close alignment between the modelled and experimental results, with minor deviations observed. During the initial phase of the test, differences appear due to the slipping of the force sensor; also, at higher displacements, slippage of the PI tensile stage occurs, attributed to the fixation of the actuator and the sample on separate boarding plates. To reduce slipping, this issue can be addressed by adding masses to the boarding plates, as shown in Figure 11.

Moving to the modelling of the magnetic circuit, expounded in Section II-C3, the results III-4 contribute

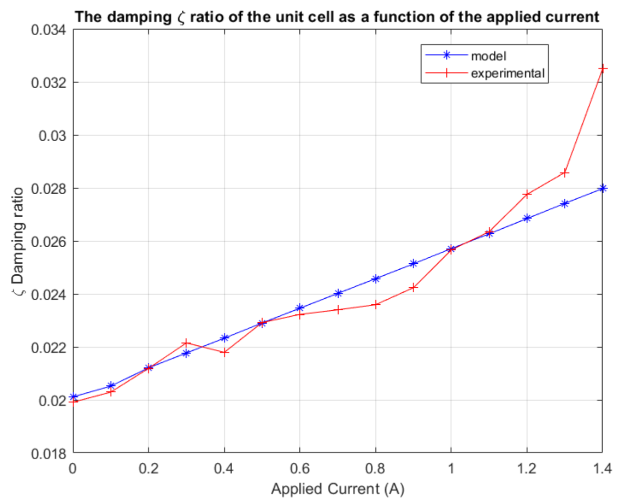


Figure 19: Modelled and experimentally estimated Damping ratio $\zeta$ as a function of the applied current

invaluable insights into the functional dynamics of the AMM unit cell. Figure 16a visually summarises the magnetic flux density within the magnetic circuit, highlighting the iron core's concentration areas and flux pathways. Meanwhile, Figure 16b provides a unique perspective by illustrating variations in magnetic flux density across the damper gap. These visualizations are instrumental in estimating the damping torque exerted at different applied currents, enhancing our understanding of the AMM unit cell's overall performance.

The simulated dynamic analysis of the AMM unit cell, executed through the developed Simulink model outlined in Section II-C4, offers valuable insights into its performance under varying magnetic flux densities. As depicted in Figure 17, the unit cell exhibits a nuanced response to different actuation current and magnetic field strength levels. The modelled unit cell dynamic, illustrated in Figure 17a, through a Bode plot diagram, provides an overview of the system's behaviour. Notably, Figure 17b zooms into the peak region of the Bode plot, revealing a distinct reduction in resonance peak amplitude with increasing applied current. This reduction signifies an augmented damping effect, showcasing the system's tunable nature. The ability to control the damping characteristics of the AMM unit cell, evident in these simulations, enhances its adaptability and performance across a range of operational scenarios.

Despite the experimentally estimated Bode plot diagram showcasing a noticeable delay in the phase plot attributed to the limitations of the laser distance sensor, this technical constraint is acknowledged. Future experiments could consider upgrading the laser distance sensor or adopting alternative measurement methods to enhance the accuracy of the phase plot. However, the observed reduction in resonance peak amplitude with increasing applied current remains a consistent and noteworthy trend. This aligns with the expectations derived from the modelled system, confirming the experimental outcomes' reliability and reinforcing the AMM unit cell's tunable and controllable nature.

A comparison between the estimated dynamic response and the modelled one described in Subsections III-5,III-6 highlights the consistency between both systems. This alignment underscores the successful execution of experimentation and analysis, providing sufficient evidence to demonstrate the tunable and controllable nature of the AMM unit cell. Additionally, Figures 18 showcase higher modes of dynamic responses, which are not associated with our unit cell. This higher mode appears when the test is conducted for the vibration shaker without attaching the unit cell.

The exploration of the damping ratio for the AMM unit cell produced valuable insights into its dynamic behaviour. Utilizing both modelled and experimentally estimated systems, the damping ratio demonstrated a tunable characteristic across varying magnetic flux densities. The close similarity between the results obtained from the modelled transfer function and the estimated system emphasises the robustness of the analytical approach. Figure 19 visually summarises this similarity. The experimental damping ratios exhibited a slight elevation for applied currents exceeding $1A$. This difference was attributed to the decrease of the damper gap.

As we look to the future, a fascinating avenue for research involves a focused exploration of miniaturization, investigating the effects and benefits of scaling down the AMM unit cell design. Furthermore, integrating these unit cells into larger lattice structures and exploring optimal orientations and configurations presents a promising path for scalable and adaptable metamaterial assemblies. Refining fabrication techniques to create structural and smart material components simultaneously is essential, considering the potential of concurrent additive manufacturing. Additionally, future investigations should delve into optimizing the structural design of the unit cell, utilizing advanced computational tools for geometry and material distribution refinement. These efforts would contribute to realizing AMMs as adaptable and efficient components in various engineering applications.

## V. Conclusion

In conclusion, this work represents a significant advancement in active mechanical metamaterials, introducing a novel unit cell design that displays tunable damping—an essential feature for various applications. The thesis includes the implementation of a magnetorheological fluid damper into an AMM unit cell for the first time to achieve tunable damping, where the AMM unit cell has been designed, modeled, built and experimentally evaluated. The results highlight the successful realization of the metamaterial unit cell with a stiffness of 1.022 kN/m and a dimension of 80 mm. The damping unit can produce tunable damping, altering the damping ratio from 0.02 to 0.03 at an applied current of 1.4A. The success of this study is evident in the convergence of theoretical predictions with experimental outcomes, emphasizing the robustness of the proposed design and modelling methodologies. The detailed insights gained from FEM analyses, experimental validations, and dynamic simulations collectively contribute to a complete understanding of the AMM unit cell's mechanical and dynamic behaviours.

Moving forward, the key novel aspects of this work lie in the successful realization of the AMM unit cell and the demonstration of its tunable damping capabilities. Future research could explore opportunities for miniaturization, investigate various lattice configurations, and refine structural designs to enhance the overall performance of active mechanical metamaterials. Additionally, integrating advanced sensing mechanisms and closed-loop control systems will further increase the adaptability and responsiveness of these metamaterials.

## VI. Acknowledgement

The author would like to thank Dr.Andres Hunt for his invaluable guidance and feedback, which significantly contributed to the refinement of this paper. Additionally, I thank Dr. Hassan Hossein Nia for his insightful insights.

## References

[1] Saravana Jothi, N. S., and A. Hunt. "Active mechanical metamaterial with embedded piezoelectric actuation." APL Materials 10.9 (2022).
[2] Kumar, Rakesh, et al. "Overview on metamaterial: History, types and applications." Materials Today: Proceedings 56 (2022): 3016-3024.
[3] Bird, Robert Byron, Robert Calvin Armstrong, and Ole Hassager. "Dynamics of polymeric liquids. Vol. 1: Fluid mechanics." (1987).
[4] Bertoldi, Katia, et al. "Flexible mechanical metamaterials." Nature Reviews Materials 2.11 (2017): 1-11.
[5] Valipour, Ali, et al. "Metamaterials and their applications: an overview." Proceedings of the Institution of Mechanical Engineers, Part L: Journal of Materials: Design and Applications (2021): 1464420721995858.
[6] Yu, Xianglong, et al. "Mechanical metamaterials associated with stiffness, rigidity and compressibility: A brief review." Progress in Materials Science 94 (2018): 114-173.
[7] Haghpanah, Babak, et al. "Programmable elastic metamaterials." Advanced Engineering Materials 18.4 (2016): 643-649.
[8] D.Thomas. "Active metamaterials: unit cells for tunable damping". Delft University of Technology, Delft (2020).
[9] Qi, Jixiang, et al. "Recent progress in active mechanical metamaterials and construction principles." Advanced Science 9.1 (2022): 2102662.
[10] Pishvar, Maya, and Ryan L. Harne. "Foundations for soft, smart matter by active mechanical metamaterials." Advanced science 7.18 (2020): 2001384.
[11] Carlson, J. D., and M. Schwartz. "Magnetorheological fluids." Smart Materials (2008): 17-1.
[12] Goncalves, Fernando D., Mehdi Ahmadian, and J. D. Carlson. "Investigating the magnetorheological effect at high flow velocities." Smart Materials and Structures 15.1 (2005): 75.
[13] Turczyn, R., and M. Kciuk. "Properties and application of magnetorheological fluids." J. Achiev. Mater. Manuf. Eng 18 (2006): 127-130.

# 4

# Conclusion

This thesis introduces a new concept in active mechanical metamaterials (AMMs) by proposing a unique unit cell design for tunable damping. The thesis includes the implementation of a magnetorheological fluid damper into an AMM unit cell for the first time to achieve tunable damping and mitigate wear that occurs due to Coulomb friction. The unit cell is designed with a structurally compliant frame, offering both stiffness and housing for the embedded MRF damper. The subsequent construction of the unit cell, coupled with analytical and experimental studies, enables a comprehensive evaluation of its mechanical effectiveness.

The study has successfully demonstrated the realization of a metamaterial unit cell with a stiffness of 1.022 kN/m and a size of 80 mm. The damping unit incorporated in the cell is capable of producing tunable damping, which can be adjusted by altering the damping ratio from 0.02 to 0.03 at an applied current of 1.4A. The detailed insights gained from FEM analyses, experimental validations, and dynamic simulations collectively provide a complete understanding of the AMM unit cell's mechanical and dynamic behaviours.

This work sets the stage for future advancements and innovations and contributes to the broader scientific community's understanding of tunable damping mechanisms. The potential applications of AMMs in various technological domains, ranging from structural engineering to vibration control, are vast and promising. The knowledge and insights from this research serve as a stepping stone for further exploration and refinement, positioning active mechanical metamaterials as a transformative force in engineering and materials science.

# 5

# Reflections and Recommendations

The pursuit of innovation and exploration in the field of mechanical metamaterials demands a multidisciplinary approach. The amalgamation of theoretical modelling, computational simulations, and experimental validations has been instrumental in uncovering the intricacies of the proposed AMM unit cell. The challenges encountered in experimental limitations or theoretical complexities have fueled a deeper understanding of the inherent complexities of designing and implementing active mechanical metamaterials. The iterative nature of the research process, wherein theoretical predictions inform experimental designs and vice versa, has been a cornerstone of the success achieved.

Based on the insights gained from this research, several recommendations emerge to guide future investigations in the realm of active mechanical metamaterials:

1. Temperature Effects: Future studies should delve deeper into the impact of temperature variations on the rheological properties of Magnetorheological Fluids (MRF). Understanding this correlation is crucial for accurately predicting and controlling the damping characteristics of AMM units.
2. Sensing and Closed-Loop Control: Embedding advanced sensing mechanisms and implementing closed-loop control systems can unlock the full potential of AMMs. This avenue of research can enhance adaptability and responsiveness, mainly when dealing with exotic material properties.
3. Miniaturizing the Design: Explore the possibilities of miniaturizing the AMM unit cell design. Investigate the effects of scaling down the unit cell to smaller dimensions and assess the potential benefits in various applications, such as micro-robotics or biomedical devices.
4. Optimizing Structural Design: Optimize the structural design of the AMM unit cell to achieve enhanced performance. Utilize advanced computational tools and optimization techniques to refine the geometry and material distribution, aiming for optimal mechanical responses under different conditions.
5. Lattice Configuration and Orientation: Investigate the feasibility of creating lattices composed of the designed unit cell. Explore optimal orientations and configurations of these lattices to harness collective mechanical properties, paving the way for scalable and adaptable metamaterial structures.
6. Fabrication Techniques: The ongoing evolution of additive manufacturing techniques presents an opportunity to refine the fabrication process of AMMs further. Future research should explore concurrent additive manufacturing of structural material and smart material actuators and sensors, streamlining the production and integration processes.
7. System Integration Strategies: As AMMs progress towards real-world applications, efficient system integration strategies become paramount. Developing methodologies to manage wiring and embedded electronics for local and global control methods will be critical for AMM technologies' scalability and practical implementation.
8. Exploration of Additional Material Properties: While this study focused on tunable damping, future investigations could explore additional material properties to broaden the application scope of AMMs.

This may include studies on tunable stiffness, shape-morphing capabilities, and multifunctional responses.

In conclusion, exploring active mechanical metamaterials represents an exciting frontier with vast potential. By addressing these recommendations and continuing to push the boundaries of knowledge, researchers can unlock new possibilities and contribute to the transformative evolution of mechanical metamaterials in engineering and materials science.

# Appendices

# A

# Detailed Technical Drawings of the unit cell

This index includes the following technical drawings:

1. The upper part of the unit cell.
2. The lower part of the unit cell.
3. The magnetic circuit.
4. The assembled unit cell.

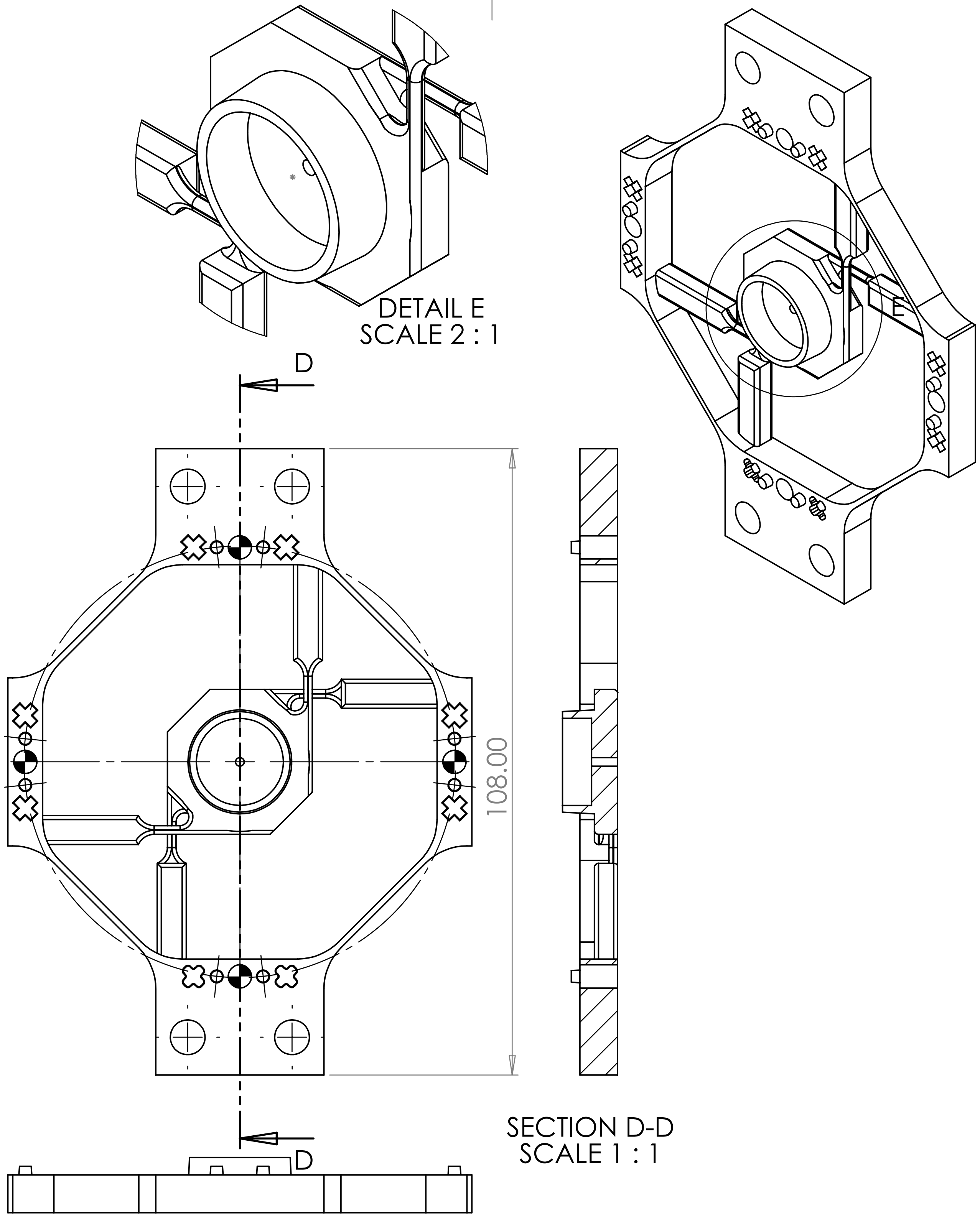


UNLESS OTHERWISE SPECIFIED:
DIMENSIONS ARE IN MILLIMETERS
SURFACE FINISH:
TOLERANCES:
LINEAR:
ANGULAR:

FINISH:

DEBURR AND BREAK SHARP EDGES

DO NOT SCALE DRAWING

REVISION

| | NAME | SIGNATURE | DATE |
|---|---|---|---|
| DRAWN | Samer Habbal | | |
| CHK'D | | | |
| APPV'D | | | |
| MFG | | | |
| Q.A | | | |

TITLE:

# Unit cell _ Upper part

MATERIAL: PETG

DWG NO.

A4

WEIGHT:

SCALE:1:2

SHEET 1 OF 1

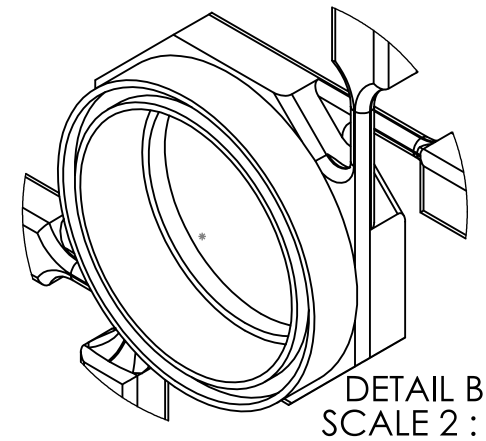

DETAIL B
SCALE 2 : 1

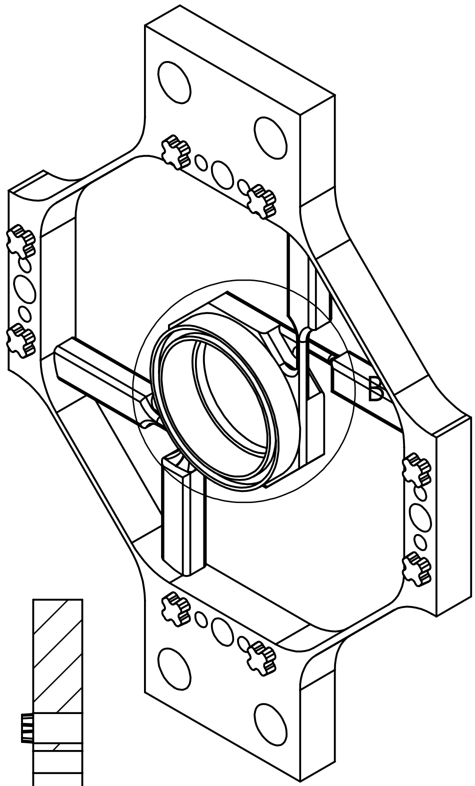


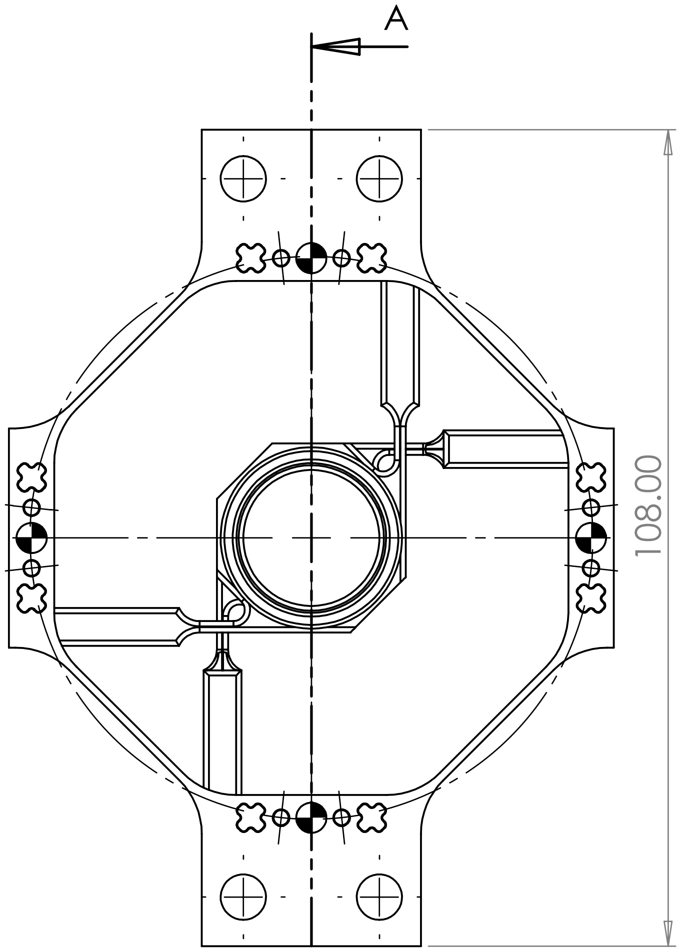


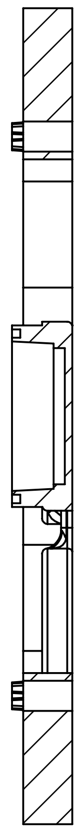

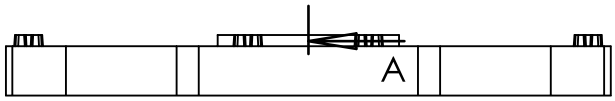

SECTION A-A
SCALE 1 : 1

UNLESS OTHERWISE SPECIFIED:
DIMENSIONS ARE IN MILLIMETERS
SURFACE FINISH:
TOLERANCES:
LINEAR:
ANGULAR:

FINISH:

DEBURR AND BREAK SHARP EDGES

DO NOT SCALE DRAWING

REVISION

| | NAME | SIGNATURE | DATE |
|---|---|---|---|
| DRAWN | Samer Habbal | | |
| CHK'D | | | |
| APPV'D | | | |
| MFG | | | |
| Q.A | | | |

TITLE:
# Unit_cell lower part

MATERIAL: PETG

DWG NO.

A4

WEIGHT:

SCALE:1:2

SHEET 1 OF 1

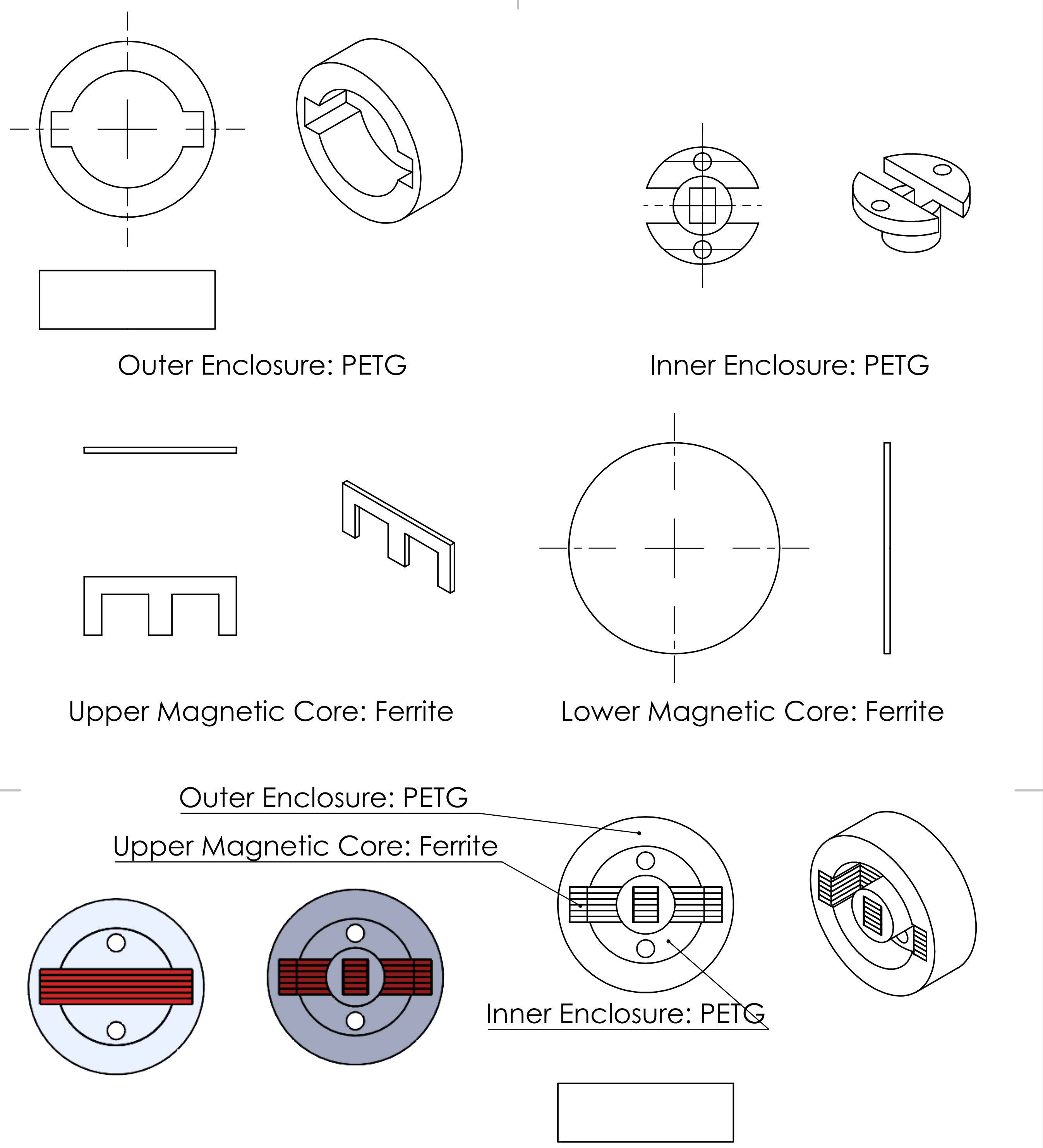


Note: The copper coil is not drwing here

| | | | | | | |
|---|---|---|---|---|---|---|
| UNLESS OTHERWISE SPECIFIED:<br>DIMENSIONS ARE IN MILLIMETERS<br>SURFACE FINISH:<br>TOLERANCES:<br>LINEAR:<br>ANGULAR: | | | FINISH: | DEBURR AND<br>BREAK SHARP<br>EDGES | DO NOT SCALE DRAWING | REVISION |
| | NAME | SIGNATURE | DATE | | TITLE: electromagnetic circuit | |
| DRAWN | Samer Habbal | | | | | |
| CHK'D | | | | | | |
| APPV'D | | | | | | |
| MFG | | | | | | |
| Q.A | | | | MATERIAL: | DWG NO. | A4 |
| | | | | WEIGHT: | SCALE:2:1 | SHEET 1 OF 1 |

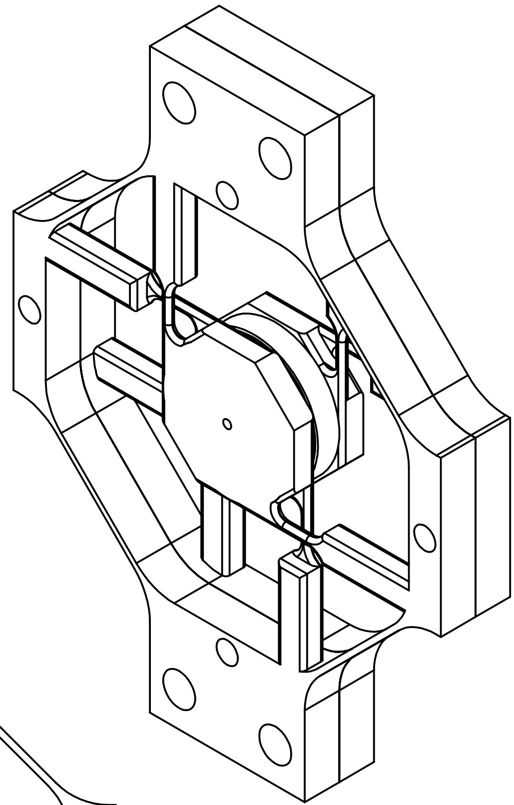

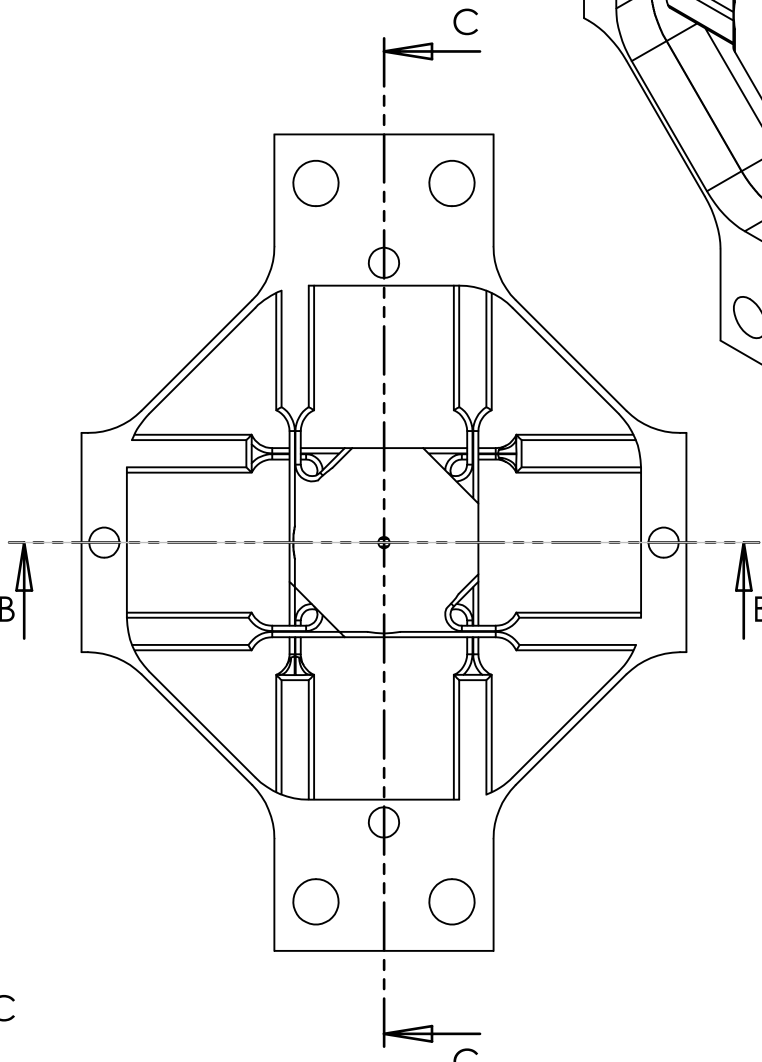


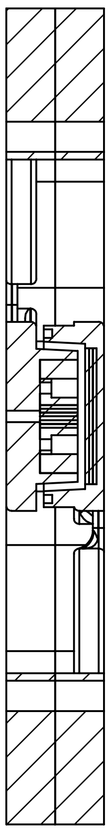

SECTION C-C
SCALE 1 : 1

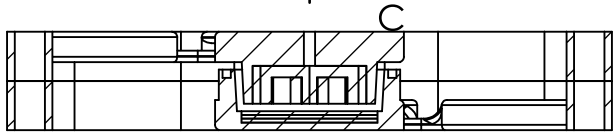

SECTION B-B
SCALE 1 : 1

| | | | |
|---|---|---|---|
| UNLESS OTHERWISE SPECIFIED:<br>DIMENSIONS ARE IN MILLIMETERS<br>SURFACE FINISH:<br>TOLERANCES:<br>LINEAR:<br>ANGULAR: | FINISH: | DEBURR AND BREAK SHARP EDGES | DO NOT SCALE DRAWING |
| | | | REVISION |

| | NAME | SIGNATURE | DATE |
|---|---|---|---|
| DRAWN | Samer Habbal | | |
| CHK'D | | | |
| APPV'D | | | |
| MFG | | | |
| Q.A | | | |

MATERIAL:

WEIGHT:

TITLE:

# Assembled unit cell

DWG NO.

A4

SCALE:1:2

SHEET 1 OF 1

# B

# Graphical Program for vibration test"Labview"

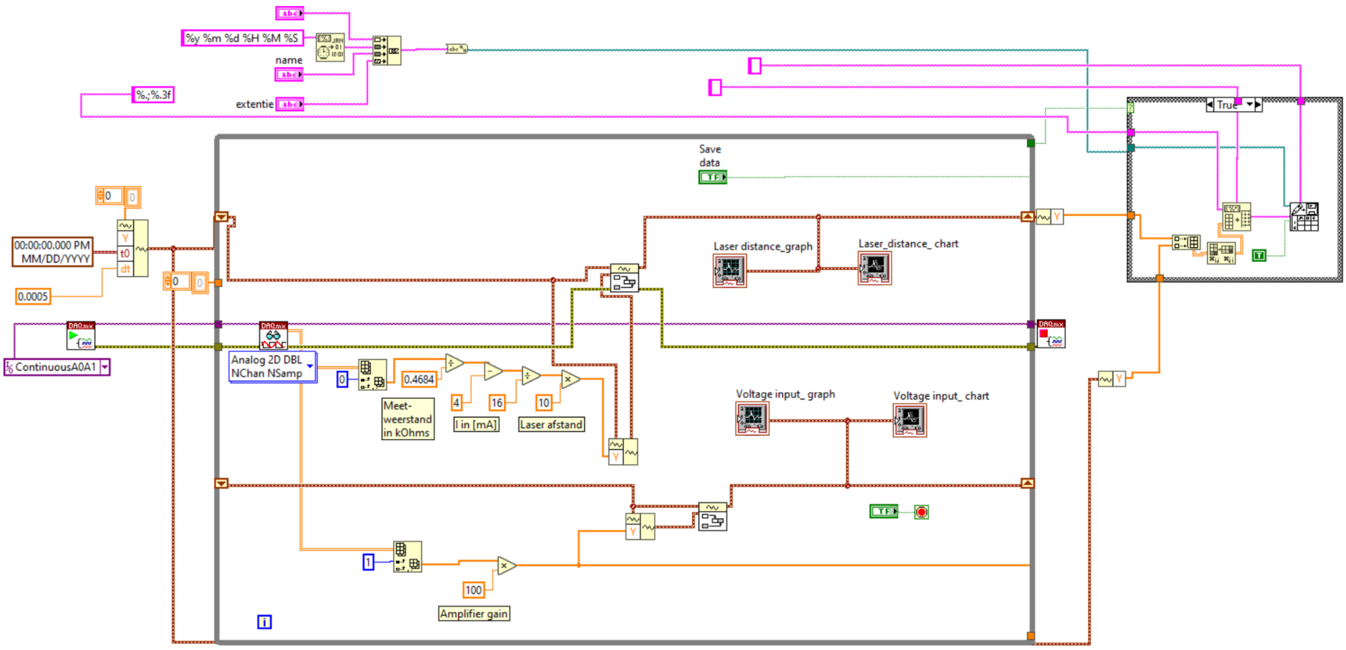


Figure B.1: Block Diagram Labview program for vibration test

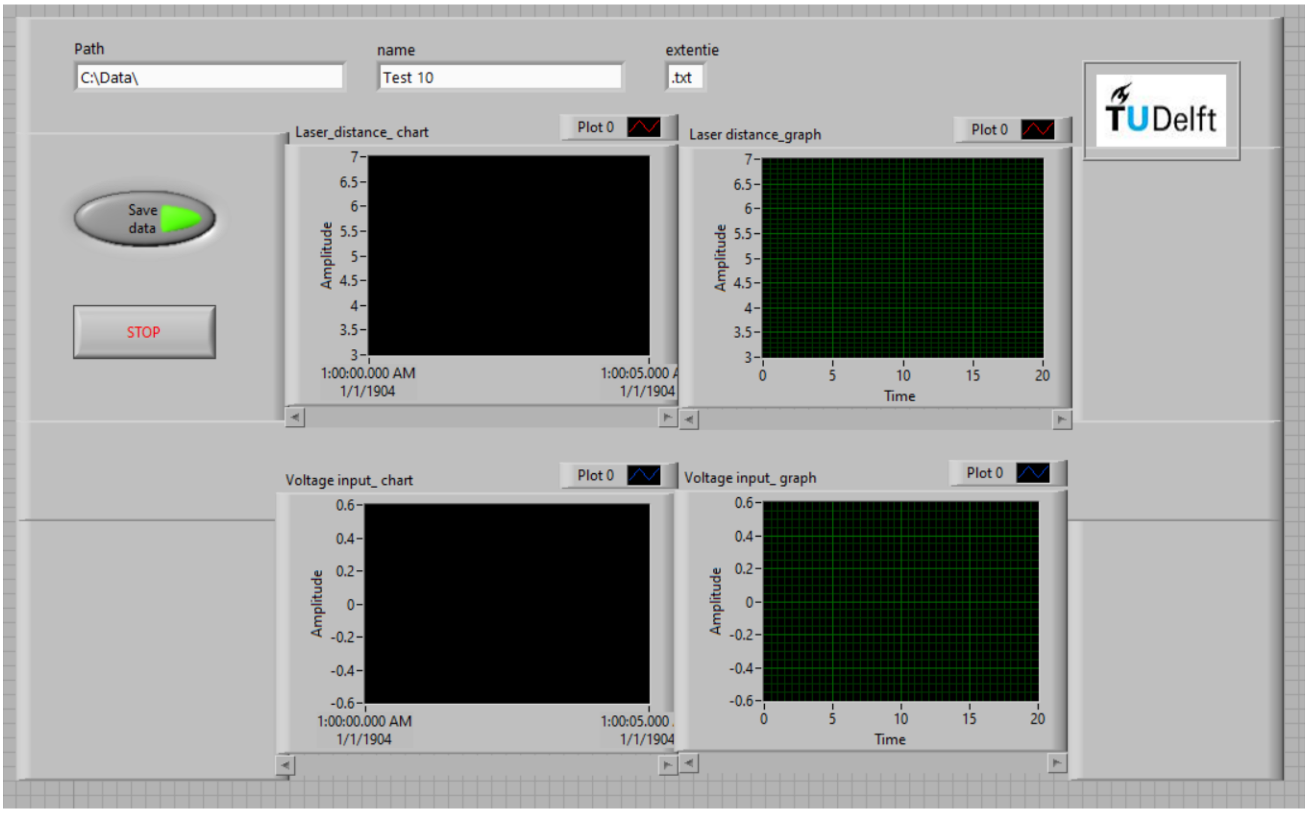


Figure B.2: Front Panel Labview program for vibration test

# C
# Supplementary files

For further details and access to supplementary materials, please email Dr. A. Hunt at A.Hunt@tudelft.nl.

The following shows a file map of the supplementary:

1. CAD Drawings.
   - Unit cell.
   - Magnetic circuit.
   - Shaker houder.
2. Modelling.
   - Simulink model of the dynamic of the unit cell.
   - FEM model of the compliant frame performance and stiffness.
   - FEM model of the magnetic circuit.
   - Magnetic flux density over the gap [Matlab].
   - MRF characterisation [Matlab].
   - Stiffness identification [Matlab].
3. Experiments and Data Analysis.
   - Data analysis and system identification [Matlab].
   - Lapview - Graphical program for vibration test.
4. Datasheets.
   - Datasheet laser optoNCDT-1420.
   - Datasheet MRF_MRHCCS4A_B_zero_field.
   - Datasheet Shaker.
5. Figures.
   - Schematic diagrams.
   - Experimental results.
   - Graphs and charts.
   - Other figures used in the report and presentation.

# Bibliography

[1] Katia Bertoldi, Vincenzo Vitelli, Johan Christensen, and Martin Van Hecke. Flexible mechanical metamaterials. *Nature Reviews Materials*, 2(11):1–11, 2017.

[2] Babak Haghpanah, Hamid Ebrahimi, Davood Mousanezhad, Jonathan Hopkins, and Ashkan Vaziri. Programmable elastic metamaterials. *Advanced Engineering Materials*, 18(4):643–649, 2016.

[3] NS Saravana Jothi and A Hunt. Active mechanical metamaterial with embedded piezoelectric actuation. *APL Materials*, 10(9), 2022.